


Occurrence and implications of secondary olivine veinlets in lunar highland breccia Northwest Africa 11273

Xiaojia ZENG ^{1,2}, Shijie LI^{1,3,*}, Katherine H. JOY⁴, Xiongyao LI^{1,2,3}, Jianzhong LIU^{1,2,3}, Yang LI^{1,2,3}, Rui LI^{1,2}, and Shijie WANG⁵

¹Center for Lunar and Planetary Sciences, Institute of Geochemistry, Chinese Academy of Sciences, Guiyang 550081, China

²Key Laboratory of Space Manufacturing Technology, Chinese Academy of Sciences, Beijing 100094, China

³CAS Center for Excellence in Comparative Planetology, Hefei, China

⁴Department of Earth and Environmental Sciences, University of Manchester, Manchester M13 9PL, UK

⁵State Key Laboratory of Environmental Geochemistry, Institute of Geochemistry, Chinese Academy of Sciences, Guiyang 550081, China

*Corresponding author E-mail: lishijielpsc@mail.gyig.ac.cn

(Received 15 December 2018; revision accepted 10 October 2019)

Abstract—Lunar breccias preserve the records of geologic processes on the Moon. In this study, we report the occurrence, petrography, mineralogy, and geologic significance of the observed secondary olivine veinlets in lunar feldspathic breccia meteorite Northwest Africa (NWA) 11273. Bulk-rock composition measurements show that this meteorite is geochemically similar to other lunar highland meteorites. In NWA 11273, five clasts are observed to host veinlets that are dominated by interconnecting olivine mineral grains. The host clasts are mainly composed of mafic minerals (i.e., pyroxene and olivine) and probably sourced from a basaltic lithology. The studied olivine veinlets (~5 to 30 μm in width) are distributed within the mafic mineral host, but do not extend into the adjacent plagioclase. Chemically, these olivine veinlets are Fe-richer ($\text{Fo}_{41.4-51.9}$), compared with other olivine grains ($\text{Fo}_{54.3-83.1}$) in lithic clasts and matrix of NWA 11273. By analogy with the secondary olivine veinlets observed in meteorites from asteroid Vesta (howardite–eucrite–diogenite group samples) and lunar mare samples, our study suggests that the newly observed olivine veinlets in NWA 11273 are likely formed by secondary deposition from a lunar fluid, rather than by crystallization from a high-temperature silicate melt. Such fluid could be sulfur- and phosphorous-poor and likely had an endogenic origin on the Moon. The new occurrence of secondary olivine veinlets in breccia NWA 11273 reveals that the fluid mobility and deposition could be a previously underappreciated geological process on the Moon.

INTRODUCTION

Since the lunar magma ocean (LMO) cooled and solidified, a variety of post-LMO processes (e.g., magmatism, volcanism, and impacts) play an important role in the Moon's geological evolution (e.g., Lucey et al. 2006; Stöffler et al. 2006). Many of these processes have formed rocks that were thought by early workers to be anhydrous in nature. However, recent re-examination of these samples using new analytical techniques has shown there to be variability of “water” (H_2O and/or OH) and other volatile elements (e.g., Saal et al. 2008; Boyce et al. 2010; Greenwood et al. 2011;

Hauri et al. 2011; Hui et al. 2013; Tartèse et al. 2013; Barnes et al. 2014; Robinson et al. 2016; Potts et al. 2018). One implication of these studies is that volatile-bearing mineral precipitation may have been commonplace within the lunar mantle, crust, and surface regolith.

Mineral assemblages and textures that are related to fluid processes in lunar samples can provide new insights into the behavior of fluid agents on the Moon, and also the volatile (e.g., F, Cl, H, and S) and chalcophile–siderophile element (e.g., Ni, Co, Cu, and Zn) transport in the lunar crust. However, the strong evidence in the lunar sample collection for fluid

processes such as fluid-driven metasomatism is, at present, relatively limited (e.g., Neal and Taylor 1991; Isa et al. 2014; Treiman et al. 2014; Warren et al. 2014). For example, the replacement texture of olivine and pyroxene by troilite documented in Apollo 16 breccias (i.e., samples 67915 and 67016) has been suggested to represent a mineralogical record of sulfur-bearing fluids on the Moon (Haskin and Warren 1991; Colson 1992; Norman et al. 1995; Shearer et al. 2012). This texture has been used to develop a thermodynamic model of S-bearing fluid in the lunar crust (Bell et al. 2015). McCallum and Schwartz (2001) suggested that Cl-rich fluid metasomatism could be a possible cause for the symplectic intergrowths of Mg-Al-chromite and two pyroxenes in igneous troctolite rock 76535, although an exogenous chromite-saturated melt was also proposed to account for this symplectite formation (Elardo et al. 2012). Lunar rock 79215 also records previously unrecognized processes in the lunar volatile cycle (i.e., impact-induced remobilization of P, F, and Cl volatiles and vapor-phase transport; Treiman et al. 2014).

More widely, the record of fluid mobility in crusts is also complex on other large planetary bodies. During the past few decades, secondary olivine veinlets (i.e., the veinlets formed of small olivine grains that crosscut pyroxene grains) have been discovered in a series of howardite-eucrite-diogenite (HED) meteorites that originated from asteroid 4-Vesta (Takeda et al. 1983, 1994; Yamaguchi et al. 1996; Warren 2002; Barrat et al. 2011; Roszjar et al. 2011; Warren et al. 2014; Mittlefehldt 2015; Pang et al. 2017; Patzer and McSween 2018). Similar secondary olivine veinlets have also been observed in a few lunar basaltic samples crosscutting pyroxene grains: these include the basaltic regolith breccia meteorite Meteorite Hills (MET) 01210 (Arai et al. 2010) and Apollo 14 mare basalts 14072 and 14310 (Roedder and Weiblen 1972; Warren et al. 2018). No secondary olivine veinlets have been reported to date in lunar highland samples. Warren et al. (2018) suggested that the olivine veinlets in Apollo basalt 14072 are likely deposited by a water-bearing fluid. However, the formation mechanism of lunar olivine veinlets and their geological records on the Moon are still poorly understood.

Northwest Africa (NWA) 11273, with a total mass of ~2.81 kg, is a newly discovered lunar feldspathic regolith breccia from Algeria in 2017 (Meteoritical Bulletin Database). The petrographic, mineralogical, and geochemical features of NWA 11273 have not been previously investigated. We have identified five olivine veinlet-bearing clasts in this meteorite. We discuss how this finding could help expand our understanding of the secondary olivine veinlets from a new geographic region on the Moon. Here, we report the detailed petrographic and mineralogical study of five olivine veinlet-bearing

clasts, and also report the bulk-rock composition and possible launch regions of NWA 11273 with the goals of interpreting the origin and geological records of the secondary olivine veinlets on the Moon.

SAMPLE AND ANALYTICAL METHODS

The NWA 11273 sample used in this study includes one 0.95 g meteorite slice provided by Eric Twelker, who has the main mass of NWA 11273, and one ~8 g specimen provided by Hao Zhu, Beijing Planetarium. This larger 8 g specimen was cut into ~1 mm thick slices by using a diamond wire saw. Seven slices were then adhered to separate 1 inch round glass slides using epoxy resin, were polished with Al₂O₃ and diamond polishing paste, coated with carbon, and investigated using different analytical techniques. The studied five sections that contain olivine veinlet-bearing clasts are shown in Fig. S1 in supporting information.

Backscattered electron (BSE) images were collected by using an FEI Scios dual-beam focused ion beam/scanning electron microscope (FIB/SEM) at Institute of Geochemistry, Chinese Academy of Sciences. The operating conditions were 15–20 kV accelerating voltage, 1.6 nA beam current, and 7 mm working distance. BSE montage maps (Figs. S2.1–S2.5 in supporting information) were stitched from multiple high-resolution BSE images (~550× magnification) using the FEI's Maps software v.3.2. These images were reviewed, and then, detailed petrography and X-ray elemental mapping (Figs. S3.1–S3.5 in supporting information) of target clasts were studied using the same FEI Scios FIB/SEM and an energy dispersive detection system (EDS of EDAX), with the same current and voltage setting noted above.

One FIB slice of NWA 11273 was prepared with the same FIB/SEM (FEI Scios) at Institute of Geochemistry, Chinese Academy of Sciences. A region of interest was first coated by an electron beam-deposited and Ga ion-deposited Pt layer. Then, a slice (15 μm × 10 μm × 170 nm) was cut by a Ga ion operated at 30 kV with beam currents ranging from 3 to 15 nA, lifted from the sample, and mounted onto a TEM copper grid. To obtain a slice with the thickness of approximately 150 nm, the Ga ion source was operated at 30 kV with beam currents in the range of 100 pA to 1 nA. Finally, a 2–5 kV ion source and 43–48 pA beam current were used for the final processing to remove the damaged surface layer. To investigate the micromorphology of this prepared FIB slice, the scanning transmission electron microscopy (STEM) micrographs were collected using the same FEI Scios FIB/SEM operating at 30 kV accelerating voltage and 0.8 nA beam current.

Quantitative major and minor element compositions of silicates (i.e., pyroxene, olivine, and plagioclase) and chromite grains (Table S1 in supporting information) were obtained using a JXA 8230 electron microprobe analysis (EMPA) at the Guilin University of Technology. This instrument was operated at an accelerating voltage of 15 kV and electron beam current of 20 nA. A peak acquisition time of 20 s (with a background measurement time of 10 s) was used for a majority of the elements analyzed (i.e., Si, Ti, Al, Cr, Fe, Mn, Mg, and Ca), with the exception of Na and K, for which a peak acquisition time of 10 s (5 s background) was used. The measurements were calibrated with well-characterized standard samples, including olivine (Si, Mg, Fe), plagioclase (Al, Na), pyroxene (Ca), mica (K), chromite (Cr), Mn-metal (Mn), and rutile (Ti). For fine-grained (<5 μm) minerals, a focused beam (<1 μm) was used, while a defocused beam of 3–5 μm was used for other large mineral grains. The typical detection limits are approximately 0.03 wt%.

An ~200 mg slice of NWA 11273 was powdered using a clean agate pestle and mortar for bulk-rock composition measurements. One powdered sample (50 mg) was dissolved in polytetrafluoroethylene-lined stainless steel bombs using a HF+HNO₃ mixture for 48 h at ~190 °C for bulk trace elements' measurements. The bulk-rock trace elements' content was analyzed using a PerkinElmer ELAN DRC-e inductively coupled plasma mass spectrometer (ICP-MS) at Institute of Geochemistry, Chinese Academy of Sciences, following standard procedures (Qi et al. 2000; Zeng et al. 2018a). Three standard reference materials (i.e., AGV-2, AMH-1, and GBPG-1; Table S2 in supporting information) were

used for analytical quality control. Rh was used as an internal standard to monitor signal drift during counting. The uncertainties (2 RSD) for most analyzed elements are 5–10%. For bulk-rock major and minor composition measurements, the other 50 mg powdered sample was analyzed by using the inductively coupled plasma optical emission spectroscopy (ICP-OES, Agilent 720) at Institute of Geochemistry, Chinese Academy of Sciences. This sample was digested with the same procedures for ICP-MS measurement and then was analyzed following the standard procedures. The analyzed elements include Ti, Al, Fe, Mn, Mg, Ca, Na, K, P, Ni, Cu, and Ba. Four standard reference materials (i.e., GSR-3, GSD-4, GSD-6, and GSR-12; Table S3 in supporting information) were used for analytical quality control. The analytical precision is better than 5% (2 RSD) for most analyzed elements.

PETROGRAPHY AND MINERALOGY OF OLIVINE VEINLET-BEARING CLASTS

Petrologic Texture

NWA 11273 is a polymict feldspathic regolith breccia meteorite that is composed of a wide range of feldspathic clasts, mineral fragments, and glass components. A BSE image of the representative region of NWA 11273 is shown in Fig. 1. In this study, five lithic clasts (i.e., clasts V1–V5; Table 1; Figs. 2 and 3) containing olivine veinlets were recognized across five different polished sections of NWA 11273 (see Figs. S1 and S2.1–S2.5). These olivine veinlets are restricted to individual clasts and do not cut across the matrix

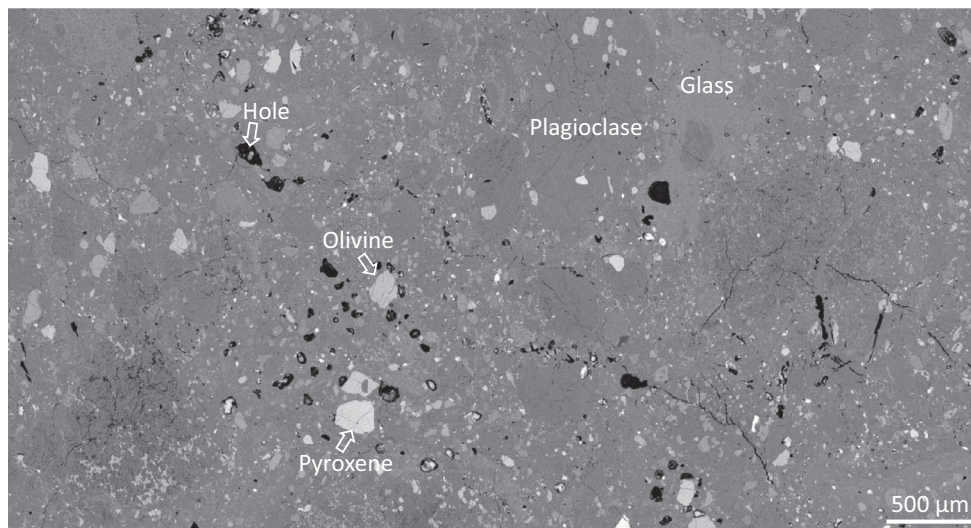


Fig. 1. Backscattered electron (BSE) image of lunar breccia NWA 11273. This meteorite is composed of a wide range of feldspathic clasts (igneous and impact origins), impact glasses, and mineral fragments. Small fractures and vesicles (black color) are found scattered through the section.

Table 1. Petrographic and mineralogical features of the clasts V1–V5 in NWA 11273.

Clast no.	Clast size (μm)	Clast textures	Primary phases of lithic clasts	Secondary olivine and associated minerals
Clast V1	1200 \times 1500	Mafic-rich clast composed of \sim 85% Px, \sim 10% Pl, $<$ 5% Chr and Tro	Px (En _{39.3-57.8} Wo _{3.0-43.5}), Pl (An _{96.9-97.5}), Chr (Chr _{59.3-62.5} Usp _{14.1}), Mer	Ol (Fa _{48.1-49.3}), Px (En _{56.7-58.9} Wo _{3.9-8.2}), Chr (Chr _{63.0-63.3} Usp _{13.1-14.6})
Clast V2	350 \times 600	Mafic-rich composed of \sim 75% Px and \sim 25% Pl with accessory Chr	Px (En _{36.2-49.5} Wo _{5.9-42.9}), Pl (An _{94.7-96.2}), Chr	Ol (Fa _{56.1-57.6})
Clast V3	120 \times 250	Pyroxene fragment with clinopyroxene exsolution	Px (En _{46.0-49.4} Wo _{7.2-14.0}), Chr	Ol (Fa _{57.1-58.6}), Pl (An _{97.2-97.6}), Chr
Clast V4	100 \times 200	Equilibrated pyroxene containing clinopyroxene grains	Px (En _{37.2-54.0} Wo _{3.7-42.0})	Ol (Fa _{54.6-56.3}), Px (En _{36.8-50.3} Wo _{7.2-42.7}), Chr (Chr _{67.7-67.8} Usp _{10.4-10.5})
Clast V5	250 \times 400	Pyroxene fragment with clinopyroxene exsolution	Px (En _{44.0-52.5} Wo _{5.1-29.2}), Pl (An _{95.7}), Chr, Tro, Mer	Ol (Fa _{52.6-54.1}), Pl (An _{96.9-97.7}), Chr

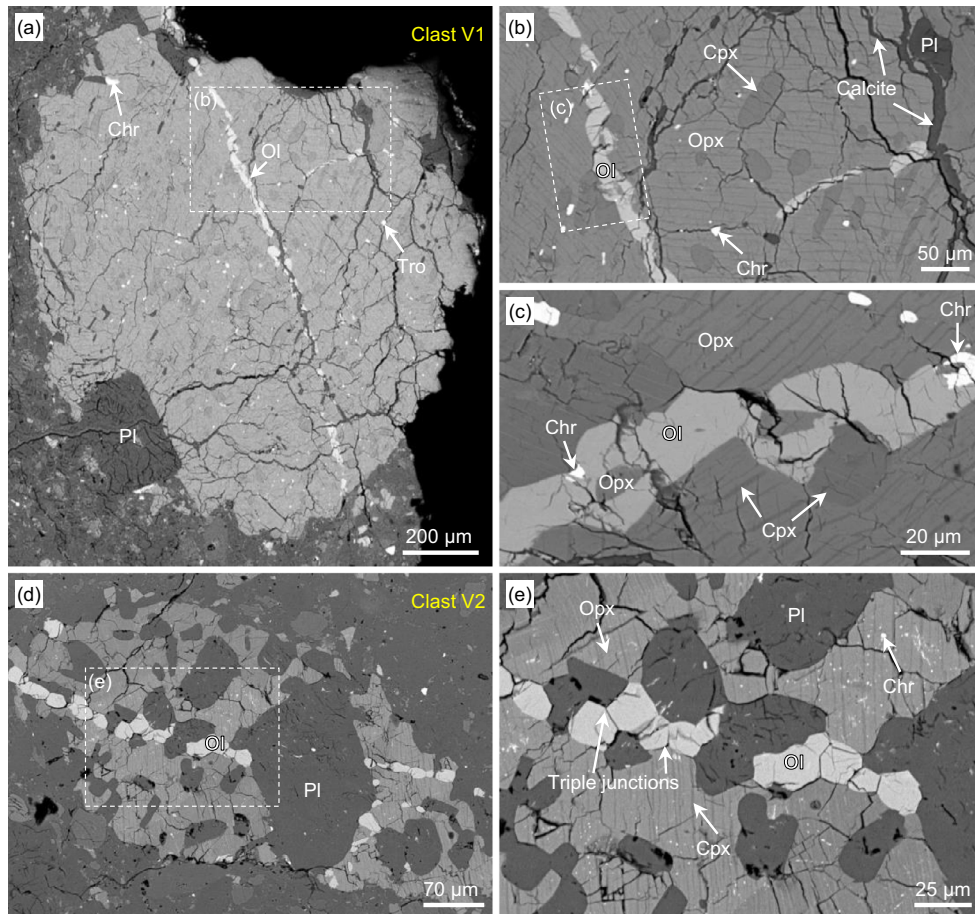


Fig. 2. BSE images of the olivine veinlet-bearing lithic clasts in NWA 11273. a) A large (up to 2 mm in length) olivine veinlet cutting across the clast V1. b, c) A close-up of the regions marked in (a), showing the detailed texture of clast V1. d) Olivine veinlets infill the pyroxene fracture in clast V2. e) Close-up image of the area marked in (d). The mineral phases are labeled: Opx = orthopyroxene, Cpx = clinopyroxene, Ol = olivine, Pl = plagioclase, Chr = chromite, Tro = troilite. (Color figure can be viewed at wileyonlinelibrary.com.)

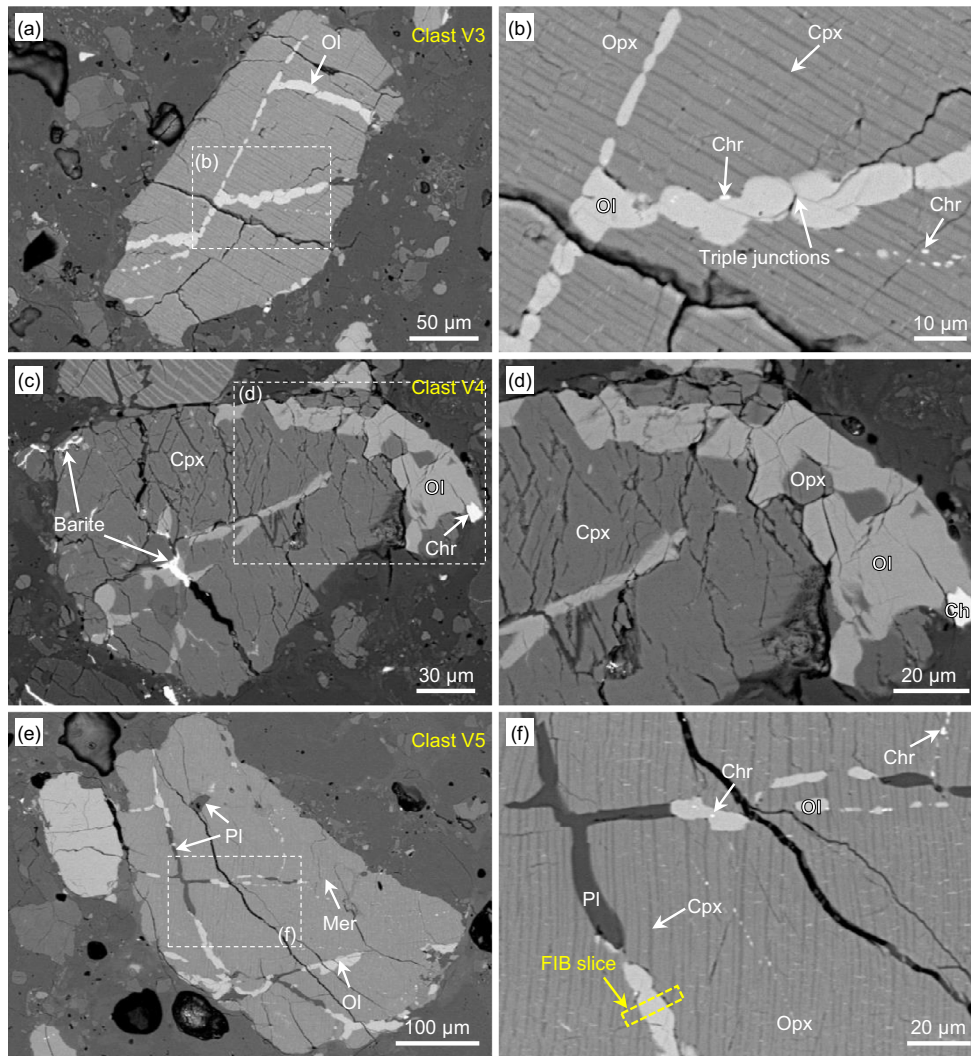


Fig. 3. BSE images of the olivine veinlet-bearing lithic clasts in NWA 11273. a) The olivine veinlets cutting through the clast V3 which exhibits exsolution clinopyroxene lamellae. b) A close-up of the region marked in (a). c) The equilibrated pyroxene fragment (clast V4) contains olivine veinlets. d) A close-up of the region marked in (c). e) A pyroxene fragment (clast V5) containing olivine veinlets. f) A close-up of the region marked in (e). The mineral phases are labeled: Opx = orthopyroxene, Cpx = clinopyroxene, Ol = olivine, Pl = plagioclase, Chr = chromite, Tro = troilite, Mer = merrillite. (Color figure can be viewed at wileyonlinelibrary.com.)

surrounding the clast. The olivine veinlets in clasts V1–V5 fill the fractures of pyroxene grains, and typically have sharp boundaries with their host pyroxene (Figs. 2 and 3). Most olivine veinlets observed in NWA 11273 are cut through by multiple fractures (e.g., Figs. 2c, 2e, 3b, and 3d). It should be noted that we did not observe the olivine veinlets occurring in other mineral phases such as plagioclase.

Clast V1 is a large (~1500 μm in size; Fig. 2a) mafic clast, mainly composed of pyroxene (~85%, by area), plagioclase (~10%), and minor (<5%) chromite and troilite grains. Pyroxene in this clast consists mainly of low-Ca pyroxene with exsolution lamellae of clinopyroxene (<3 μm in width; Fig. 2c). Fine-grained (<10 μm) chromite grains

are scattered within this clast. Two olivine veinlets were observed cutting across pyroxene grains with the width of ~25 μm (Fig. 2b). Smaller (<20 μm) grains of low-Ca pyroxene and chromite are detected in close association with the olivine veinlet (Fig. 2c).

Clast V2 is another olivine veinlet-bearing mafic-rich clast that mainly consists of ~75% pyroxene with ~25% plagioclase (Fig. 2d). The olivine veinlets (~25 μm in width) cut across the pyroxene crystal and did not cut across the plagioclase grains in these clasts (Fig. 2d). The host low-Ca pyroxene contains thin (<3 μm in width) lamellae of clinopyroxene (Fig. 2e). Most olivine grains in this veinlets show ~120° triple junction grain boundaries (Fig. 2e).

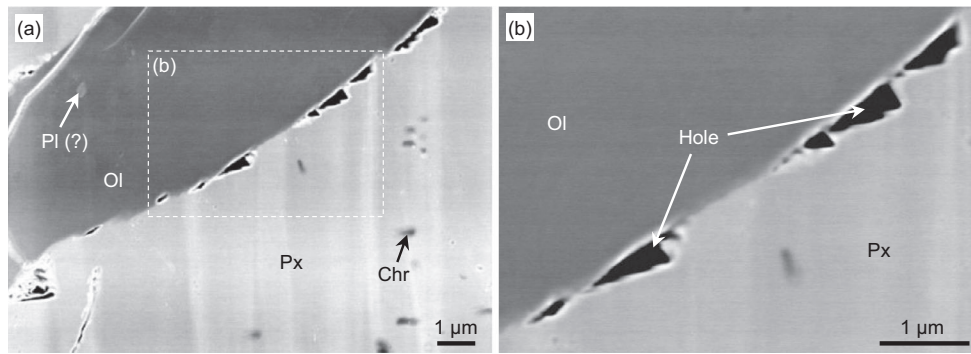


Fig. 4. The STEM image of secondary olivine veinlet in clast V5 (Fig. 3f), with close-up view of the contact shown in (b). Px = pyroxene, Ol = olivine, Chr = chromite, Pl = plagioclase.

In addition to the mafic clasts V1 and V2, olivine veinlets were also observed in three pyroxene fragments (i.e., clasts V3–V5; Fig. 3) in NWA 11273. Clast V3 is about 250 μm in size and is cut by irregular olivine veinlets with a width of 3–10 μm (Fig. 3a). This pyroxene fragment contains thin (<2 μm) exsolution lamellae of clinopyroxene. A few chromite grains are observed in the olivine veinlets in clast V3 (Fig. 3b). One low-Ca pyroxene fragment (i.e., clast V4) has an irregular clast boundary (~200 μm in size) and does not contain the clinopyroxene exsolution lamellae. Several olivine veinlets (~10 to ~35 μm in width) are found within and surrounding this fragment (Fig. 3c). The small (<15 μm) grains of pyroxene and chromite are presented within the olivine veinlets of Clast V4 (Fig. 3d). Clast V5 is a large (~250 \times 400 μm in size; Fig. 3e) pyroxene containing several irregular olivine and plagioclase veinlets (~10 μm in width) that cut across this clast. This host low-Ca pyroxene contains thin (<2 μm) exsolution lamellae of clinopyroxene and also a few small plagioclase, troilite, and merrillite grains (Fig. 3f). A few chromite grains are observed in both olivine veinlets and the host pyroxene crystal (Fig. 3f).

STEM Observations

The boundaries between secondary olivine veinlets and their host pyroxene could help us to understand the formation mechanism of olivine veinlets. To observe the micromorphology between secondary olivine veinlets and their host pyroxene, an FIB section of 15 \times 10 μm was extracted from clast V5 (see Fig. 3f). The STEM image shows that the olivine veinlets have distinct boundaries with their host pyroxene grains (Fig. 4). No replacement texture of pyroxene by olivine was observed at submicron scale. The pyroxene grains show serrated grain boundary, resulting in the wedge-shaped hole with a length of ~1 μm (Fig. 4b). Such

microstructures more likely represent the brittle fracture of pyroxene (e.g., see also similar textures in rocks from the terrestrial Lockne impact crater, Sweden; fig. 3 of Agarwal et al. 2017).

Mineral Composition

The mineral compositions for lithic clasts V1–V5 in NWA 11273 are provided in Tables S1 and S2. Both secondary olivine veinlets and their host pyroxene in clasts V1–V5 have Fe-Mn (atomic) trends similar to the Fe-Mn trends for other olivine and pyroxene in the rest of the NWA 11273 meteorite and Apollo returned samples (Fig. 5).

The pyroxene in lithic clasts and matrix of NWA 11273 have a large composition variation (i.e., $\text{En}_{13.2-80.5}\text{Fs}_{6.9-59.2}\text{Wo}_{2.5-47.6}$; Fig. 6a). In comparison, the olivine veinlet-host pyroxene grains in clasts V1–V5 show relatively smaller composition ranges (i.e., $\text{En}_{35.0-58.9}\text{Fs}_{17.1-46.9}\text{Wo}_{3.0-43.5}$; Figs. 6b–d). In particular, pyroxene grains in clasts V1–V5 have relatively small Mg# (Mg# = atomic $100 \times \text{Mg}/[\text{Mg}+\text{Fe}]$) ranges of 52.5–69.7, while other pyroxene in NWA 11273 (including lithic clasts and matrix) have large Mg# variation (i.e., Mg# = 18.2–86.8; Fig. 7; Table S1). The plagioclase grains in clasts V1–V5 are calcic and have small composition variation (i.e., $\text{An}_{94.7-97.7}$), which are in the range of An values for other plagioclase grains in NWA 11273 (Fig. 7).

In clasts V1–V5, the mineral fragments (i.e., plagioclase and chromite) associated with the olivine veinlets have similar chemical compositions to other plagioclase and chromite grains that are hosted within the parent clast (Table 2). The olivine veinlets in clasts V1–V5 show relatively small compositional variation (Fig. 7). Specifically, the olivine grains in clast V1 are relatively Mg-rich (i.e., $\text{Fa}_{48.1-49.3}$), while the olivine grains in clasts V2–V5 are relatively Fe-rich, that is, $\text{Fa}_{56.1-57.6}$ for clast V2, $\text{Fa}_{57.1-58.6}$ for clast V3, $\text{Fa}_{54.6-56.3}$

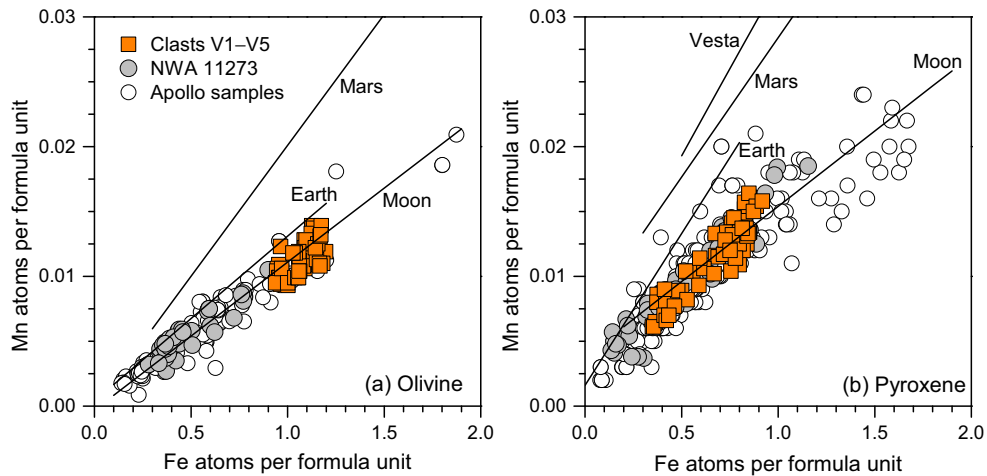


Fig. 5. Fe-Mn contents in olivine (a) and pyroxene (b) of clasts V1–V5 (orange squares), compared with the Fe-Mn contents in olivine and pyroxene for NWA 11273 (including lithic clasts and matrix; gray circles) and Apollo samples (open circles; Joy et al. [2014] and references therein). Planetary trend lines for Earth, Mars (Martian meteorites), and Vesta (HED meteorites) are from Papike et al. (2009). (Color figure can be viewed at wileyonlinelibrary.com.)

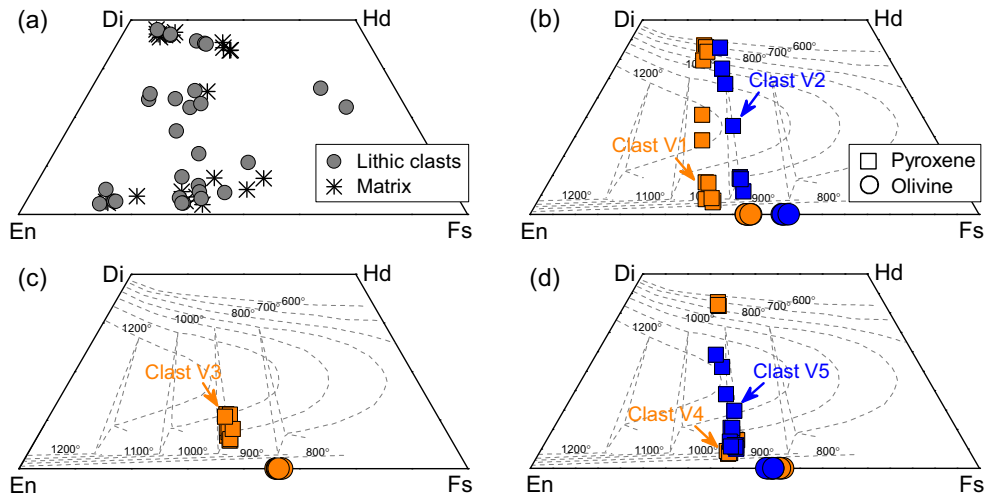


Fig. 6. (a) Quadrilateral pyroxene composition of lithic clasts and matrix minerals in NWA 11273. b–d) Quadrilateral pyroxene compositions of clasts V1–V5. Olivine Fo compositions are shown on the x -axis. Some of the pyroxene compositions (with intermediate Wo-values) appear to be a mixture of orthopyroxene and clinopyroxene. Two-pyroxene thermometer boundaries were taken from Lindsley and Andersen (1983). Considering the thin ($<2 \mu\text{m}$) exsolution lamellae of clinopyroxene, some of the pigeonitic compositions are likely a mixture of orthopyroxene and clinopyroxene analyses. (Color figure can be viewed at wileyonlinelibrary.com.)

for clast V4, and $\text{Fa}_{52.6-54.1}$ for clast V5 (Table 1). Compared with other olivine grains in NWA 11273 (including lithic clasts and matrix) that have the Mg# values ranging from 54.3 to 83.1, these olivine veinlets in clasts V1–V5 obviously have relatively lower Mg# values of 41.4–51.9 (Fig. 7).

BULK-ROCK METEORITE COMPOSITION

The bulk-rock major, minor, and trace element composition of NWA 11273 is listed in Table 3. This

meteorite has bulk Al_2O_3 and FeO contents of 25.1 and 4.35 wt%, respectively (Table 3), similar to the Apollo 16 soils (Lucey et al. 2006) and lunar feldspathic meteorites (see comparison in Fig. 8a). The CI-normalized (Anders and Grevesse 1989) rare earth elements (REE) pattern of NWA 11273 shows lower REE abundance ($5 \times \text{CI La}$, $3 \times \text{CI Lu}$; Fig. 8b) compared with Apollo 16 typical mature soils and the average lunar feldspathic highland crust (Fig. 8b). Compared with the Apollo 16 regolith samples that generally have Sm >2 ppm and Th >1 ppm (e.g.,

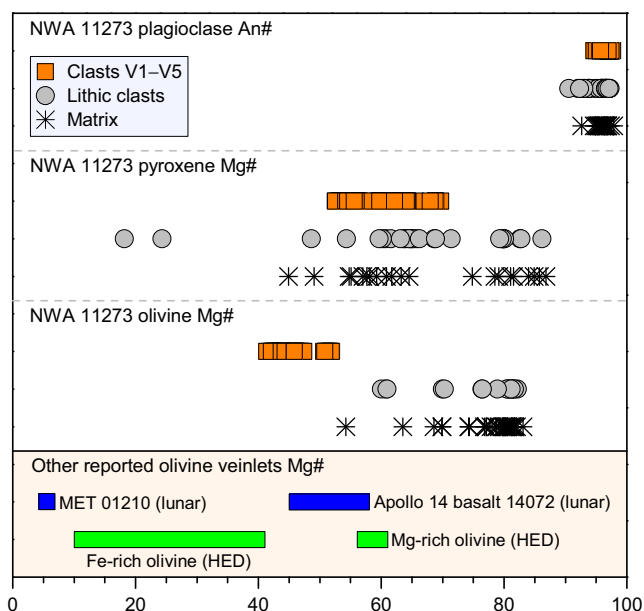


Fig. 7. Mafic minerals (i.e., pyroxene and olivine) Mg# ranges and plagioclase An# ranges for clasts V1–V5, compared to those for other lithic clasts and matrix of NWA 11273. The Mg# of olivine veinlets in Apollo mare basalt 14072 (Warren et al. 2018), lunar regolith breccia meteorite Hills (MET) 01210 (Arai et al. 2010), and HED meteorites (Barrat et al. 2011; Roszjar et al. 2011; Warren et al. 2014; Pang et al. 2017) are also shown for comparison. (Color figure can be viewed at wileyonlinelibrary.com.)

Korotev 1997), NWA 11273 has relatively lower concentrations of incompatible trace elements (e.g., Sm = 0.49 ppm and Th = 0.17 ppm; Table 3).

REMOTE SENSING DATA AND POTENTIAL LAUNCH REGIONS

Remote sensing missions provide key insights to the geochemical diversity of the Moon. For example, the Lunar Prospector mission gamma ray spectrometer (LP-GRS) has measured the abundance of rock-forming and radioactive incompatible elements (e.g., O, Si, Fe, Ti, Mg, Al, Th, and K) within tens of centimeters of the lunar surface (Binder 1998). In addition, bulk-rock composition of lunar regolith breccia meteorites also extend our understanding of the geochemistry of lunar surface (i.e., few centimeters to meters) materials, where the meteorites ejected from (Lorenzetti et al. 2005; Joy et al. 2010; Calzadiaz et al. 2015). Measurements of Apollo samples and lunar meteorites shown that bulk-rock FeO and Th contents have been used to help identify (distinguish) different lithologies on the Moon (e.g., fig. 17 of Korotev 2005). Specifically, lunar highland feldspathic-rich materials are characterized by relative

low abundance of FeO and low ITEs (e.g., Th), while mafic-rich basaltic lithologies exhibit high content of FeO and high ITEs (e.g., Th). Therefore, by comparing bulk-rock composition of regolith breccia meteorites with LP-GRS geochemical data (i.e., FeO and Th), the meteorite's likely launch location(s) can be constrained.

In this work, we used the bulk FeO (4.35 ± 1 wt%) and Th (0.17 ± 1 ppm) contents of NWA 11273 as input parameters to locate regoliths with similar compositions following the method reported in Joy et al. (2010) and Zeng et al. (2018a). The resulting map (Fig. 9) shows that NWA 11273 is compositionally similar to the regolith in the anorthositic-Feldspathic Highland Terrane (FHT-An), and also to regolith around the FHT-An in the outer-Feldspathic Highland Terrane (FHT-O).

DISCUSSION

Lunar Origin of the Olivine Veinlet-Bearing Clasts V1–V5

Although exogenic mineral and lithic components (e.g., chondrite and iron meteorites) could be preserved in polymict lunar breccias (e.g., Day et al. 2006; Joy et al. 2012, 2016), the mineralogy of clasts V1–V5 suggest that these clasts have a lunar origin. Evidence includes that (1) the anorthitic nature of plagioclase ($An_{94.7-97.7}$; Fig. 6) in clasts V1–V5 is consistent with that of lunar samples (e.g., Korotev 2005; Sokol et al. 2008); and (2) both the olivine veinlets and their host pyroxenes have the Fe-Mn (atomic) trends similar to the typical Fe-Mn trends for NWA 11273 lithologies and matrix as well as other lunar samples (Fig. 5; Papike et al. 2009; Joy et al. 2014), which are suggestive of a lunar origin.

NWA 11273 is a hot desert meteorite that could be contaminated by weathering processes on the Earth (Lee and Bland 2004; Saunier et al. 2010; Velbel 2014). Previous studies demonstrated that the terrestrial weathering can modify the mineralogical and geochemical information of desert meteorites; the weathering products commonly include calcite (e.g., Fig. 2b), barite (e.g., Fig. 3c), Fe-oxides, and clay, but do not include olivine grains (Lee and Bland 2004; Al-Kathiri et al. 2005; Saunier et al. 2010; Hyde et al. 2014; Velbel 2014). This suggests that the olivine veinlets in clasts V1–V5 are not likely terrestrial weathering products. In addition, the olivine veinlets in NWA 11273 were observed to be cut through by multiple fractures (probably induced by shock events); see Figs. 2c, 2e, 3b, and 3d), suggesting that these veinlets were formed before this meteorite was ejected off the Moon and/or fell to the Earth.

Table 2. Representative mineral composition of the clasts V1–V5 in NWA 11273. Full data are provided in Table S1.

	Clast V1 ^a						Clast V2 ^a				
	Ol	Px	Px*	Pl	Chr	Chr*	Ol	Px	Pl		
SiO ₂	35.0	35.3	50.0	53.0	43.4	0.32	0.32	34.6	51.5	50.8	43.1
TiO ₂	b.d.	0.06	0.48	0.18	b.d.	5.04	5.35	0.08	0.30	0.47	b.d.
Al ₂ O ₃	b.d.	0.05	1.45	0.41	34.8	10.7	10.4	0.03	0.45	0.81	34.1
Cr ₂ O ₃	b.d.	0.07	0.43	0.14	b.d.	42.4	44.2	b.d.	0.15	0.26	b.d.
FeO	39.9	39.4	11.0	23.3	0.15	36.6	34.7	45.0	25.9	21.0	0.39
MnO	0.41	0.39	0.19	0.38	b.d.	0.05	0.20	0.45	0.43	0.41	0.03
MgO	23.9	23.8	14.2	20.7	0.05	2.59	2.87	19.6	16.8	15.1	0.25
CaO	0.19	0.31	21.7	1.91	21.1	0.09	0.15	0.21	4.39	11.0	20.8
Na ₂ O	0.05	0.10	0.05	0.03	0.35	0.05	0.08	b.d.	0.03	0.07	0.53
K ₂ O	b.d.	b.d.	b.d.	b.d.	b.d.	0.24	b.d.	b.d.	b.d.	0.03	0.11
Total	99.44	99.55	99.47	100.1	99.95	98.02	98.27	99.90	99.96	99.86	99.28
Mg#	51.6	51.9	69.7	61.3				43.7	53.6	56.1	
Fa	48.4	48.1						56.3			
En			39.4	58.9		Chr (62.5)	Chr (63.3)		48.7	43.4	
Fs			17.1	37.2		Hc (23.4)	Hc (22.1)		42.2	33.9	
Wo			43.5	3.9		Usp (14.1)	Usp (14.6)		9.2	22.7	
An					97.0						95.0

	Clast V3 ^a			Clast V4				Clast V5 ^a			
	Ol	Px	Pl*	Ol	Px	Px*	Chr*	Ol	Px	Pl	Pl*
SiO ₂	34.9	51.4	42.0	37.1	51.6	51.5	0.12	34.5	51.8	44.4	43.3
TiO ₂	b.d.	0.16	b.d.	0.06	0.20	0.20	3.81	b.d.	0.21	b.d.	0.04
Al ₂ O ₃	0.09	0.47	34.5	0.11	0.92	0.47	10.1	0.04	0.54	35.4	33.8
Cr ₂ O ₃	0.04	0.39	b.d.	0.07	0.37	0.14	46.9	0.03	0.18	b.d.	b.d.
FeO	44.3	25.8	1.15	41.9	13.0	25.5	34.9	43.6	26.6	0.68	1.25
MnO	0.52	0.46	b.d.	0.39	0.28	0.48	0.04	0.46	0.41	b.d.	b.d.
MgO	18.6	16.9	0.56	19.6	13.0	17.0	2.34	21.0	17.7	0.04	0.28
CaO	0.97	4.03	21.1	0.52	20.50	3.40	0.21	0.23	2.43	20.9	20.7
Na ₂ O	0.08	0.04	0.26	b.d.	0.06	0.03	0.04	b.d.	0.03	0.47	0.34
K ₂ O	b.d.	0.10	0.11	0.04	b.d.	b.d.	0.05	b.d.	b.d.	0.07	0.05
Total	99.54	99.84	99.65	99.71	99.92	98.68	98.52	99.83	99.92	101.9	99.80
Mg#	42.9	53.9		45.4	64.1	54.2		46.2	54.3		
Fa	57.1			54.6				53.8			
En		49.4			37.2	50.3	Chr (67.8)		51.5		
Fs		42.2			20.8	42.4	Hc (21.8)		43.4		
Wo		8.4			42.0	7.2	Usp (10.5)		5.1		
An			97.2							95.7	96.9

b.d. = below detection limit; Ol = olivine; Px = pyroxene; Px* = pyroxene grains within the secondary olivine; Pl* = plagioclase grains within the secondary olivine; Pl = plagioclase, Chr = chromite, Chr* = chromite grains within the secondary olivine, Spl = Usp = ulvospinel, Hc = hercynite.

^aConsidering the thin (<2 μm) exsolution lamellae of clinopyroxene, the reported clinopyroxene composition could be collected from a mixture of orthopyroxene and clinopyroxene.

Host Rock of the Olivine Veinlet-Bearing Clasts V1–V5

Mineralogically, clasts V1–V5 are mafic rich predominately composed of pyroxene with minor plagioclase and accessory chromite grains (Figs. 2 and 3). This suggests that clasts V1–V5 are not like plagioclase-rich lunar highland crustal rocks (e.g., the anorthosite and feldspathic impact-melt clasts; Cahill et al. 2004; Yamaguchi et al. 2010; Wittmann et al.

2014), but are more similar to basaltic lithologies found in other lunar breccia meteorites (e.g., Snape et al. 2011; Mercer et al. 2013; Joy et al. 2014). This conclusion is further supported by the mineral composition of these clasts (Fig. 10): clasts V1–V5 have pyroxene compositions (i.e., Fe# and Ti) similar to pyroxene from Apollo low-titanium (Low-Ti) and very low-titanium (VLT) basalts (Fig. 10). We note that the variation of Fe# is relatively small within individual lithic clasts,

Table 3. Bulk-rock composition of NWA 11273, compared with the calculated average composition of the feldspathic lunar crust and typical mature nearside highland (Apollo 16) soils.

NWA 11273		Feldspathic crust Korotev et al. (2003)	Apollo 16 soils Lucey et al. (2006)
ICP-OES ^a (2SD)	ICP-MS ^b (2SD)		
<i>Major and minor elements (wt%)</i>			
SiO ₂	n.d.	44.7	44.9
TiO ₂	0.17	0.22	0.59
Al ₂ O ₃	25.10 ± 0.11	28.2	26.7
Cr ₂ O ₃	n.d.	0.096	0.111
FeO	4.35 ± 0.06	4.4	5.44
MnO	0.06	0.063	0.07
MgO	7.04 ± 0.13	5.4	6
CaO	15.0 ± 0.13	16.3	15.3
Na ₂ O	0.39 ± 0.01	0.35	0.46
K ₂ O	0.03	0.027	0.121
P ₂ O ₅	0.04 ± 0.02		0.12
Total		99.8	99.9
Mg#	74.3	69	66
<i>Trace elements (ppm)</i>			
Li	4.32 ± 0.86		8
Be	0.11 ± 0.32		
Sc	6.38 ± 0.21	8	9.5
V	21.7 ± 0.69		25
Cr	662 ± 33.8		760
Co	18.0 ± 0.5	17	31
Ni	137 ± 6.31	185	440
Cu	4.45 ± 3.08		
Zn	6.79 ± 0.16		26
Ga	2.74 ± 0.19		3.6
Ge	0.21 ± 0.08		
As	0.51 ± 0.14		
Rb	0.55 ± 0.03		2.9
Sr	168 ± 1.15	150	176
Y	4.72 ± 0.19		46
Zr	14.9 ± 0.5		180
Nb	1.05 ± 0.01		13
Mo	0.04 ± 0.02		
Ag	0.03 ± 0.03		
Cd	0.03 ± 0.03		
Sn	0.23 ± 0.01		
Cs	0.03 ± 0.01		0.14
Ba	137 ± 25.9		140
La	1.12 ± 0.04	2.3	13
Ce	2.92 ± 0.15	6	34
Pr	0.38		4.5
Nd	1.85 ± 0.09		21
Sm	0.49 ± 0.13	1.1	6
Eu	0.77 ± 0.11	0.78	1.2
Gd	0.72 ± 0.07	1.3	8
Tb	0.12 ± 0.02	0.23	1.2
Dy	0.84 ± 0.09		8
Ho	0.18 ± 0.02		1.7

Table 3. *Continued.* Bulk-rock composition of NWA 11273, compared with the calculated average composition of the feldspathic lunar crust and typical mature nearside highland (Apollo 16) soils.

NWA 11273		Feldspathic crust Korotev et al. (2003)	Apollo 16 soils Lucey et al. (2006)
ICP-OES ^a (2SD)	ICP-MS ^b (2SD)		
Er	0.52 ± 0.03		5
Tm	0.08 ± 0.02		0.7
Yb	0.51 ± 0.05	0.89	4.3
Lu	0.07 ± 0.01	0.13	0.61
Hf	0.36 ± 0.05	0.8	4.5
Ta	0.07 ± 0.02	0.11	0.55
W	1.36 ± 0.42		0.5
Pb	0.33 ± 0.02		
Th	0.17 ± 0.02	0.37	2.22
U	0.08 ± 0.01		0.62

^aDetermined by ICP-OES for a 50 mg powder sample.

^bDetermined by ICP-MS for a 50 mg powder sample.

Errors reported are two standard deviations on the basis of three repeat measurements. n.d. = not determined.

while Ti# shows relatively large variation. Such a chemical trend could be caused by different diffusion rates of these elements (i.e., the Fe and Mg have faster diffusion rates than that for Ti and Cr; Arai et al. 1996; Zhang and Hsu 2009; Fagan et al. 2014). This difference makes Fe# more easily homogenized than Ti# in pyroxene when the subsequent annealing processes occur (Arai et al. 1996). Such geochemical character (i.e., Fe# and Ti# trend) suggests that the host rock of clasts V1–V5 underwent postmagmatic re-equilibration. This interpretation is strongly supported by the exsolution texture observed in these clasts (i.e., clasts V1, V2, V3, and V5; Figs. 2 and 3).

The olivine veinlet-bearing clasts V1–V5 show a variety of petrographic texture and mineralogy. For example, (1) clast V1 distinctively contains oval-shaped high-Ca pyroxene, (2) clast V2 distinctively contains rounded plagioclase grains, and (3) clast V4 distinctively contains no exsolution lamellae at microscale. These features indicate that clasts V1–V5 might represent at least three different parent rocks and clearly experienced different formation histories as well.

Origin of Secondary Olivine Veinlets in NWA 11273: Fluid Deposition?

The secondary olivine veinlets that cut across pyroxene grains have been previously observed in several of HED meteorite samples (Takeda et al. 1983,

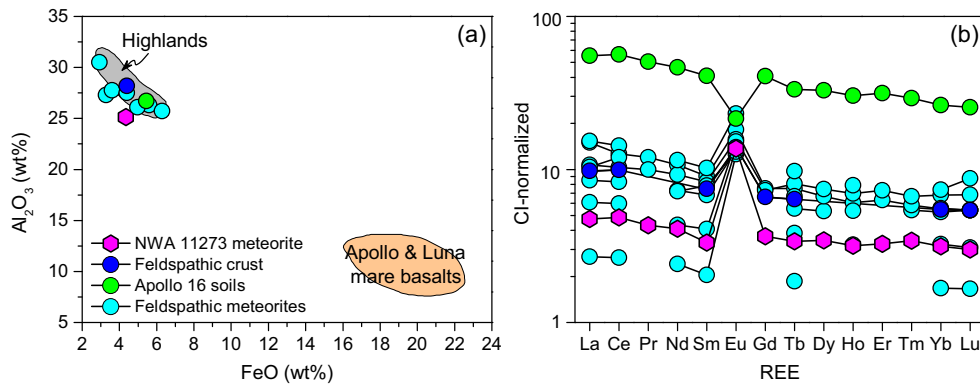


Fig. 8. Bulk-rock composition of NWA 11273. a) Bulk composition of Al_2O_3 versus FeO in NWA 11273 (Table 3), compared with other reported lunar feldspathic meteorites (cyan circles; these meteorites are ALHA 81005, Dhofar 489, DaG 400, PCA 02007, Dhofar 025, Dhofar 081, and DaG 262; Laul et al. [1983]; Cahill et al. [2004]; Warren et al. [2005]; Korotev et al. [2006]; Joy et al. [2010]), feldspathic crust (Korotev et al. 2003), and Apollo 16 typical mature soils (green circle; Lucey et al. 2006). The highlands and mare regions are taken from Korotev et al. (2003). (b) The CI-normalized (Anders and Grevesse 1989) REE pattern of NWA 11273 (Table 3) compared with the lunar feldspathic meteorites, average feldspathic crust (Korotev et al. 2003), and average Apollo 16 soils (Lucey et al. 2006). (Color figure can be viewed at wileyonlinelibrary.com.)

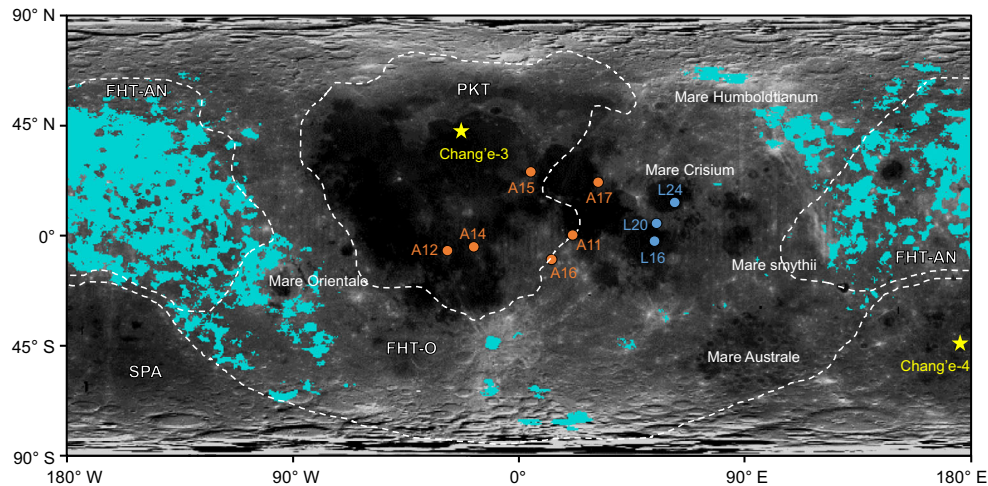


Fig. 9. Compositional constraints of likely launch regions of NWA 11273 using the Lunar Prospector $0.5^\circ/\text{pixel}$ FeO (wt%) and Th (ppm) data sets (Lawrence et al. 2002, 2003). The cyan areas are compositional similar regoliths to the composition of NWA 11273 (i.e., $\text{Fe} = 4.35 \pm 1$ wt%, $\text{Th} = 0.17 \pm 1$ ppm; Table 3). Locations of the Apollo and Luna sample return missions are noted, along with the Chang'e-3/Chang'e-4 lander and rover landing site. The map highlights with dashed outlines the main geochemical terranes defined by Jolliff et al. (2000). (Color figure can be viewed at wileyonlinelibrary.com.)

1994; Barrat et al. 2011; Roszjar et al. 2011; Mittlefehldt et al. 2013; Warren et al. 2014; Pang et al. 2017; Patzer and McSween 2018), and also in a few basaltic lunar samples (i.e., the Apollo 14 basalt 14072 and the basaltic breccia meteorite MET 01210; Arai et al. 2010; Warren et al. 2018). Two types of olivine veinlets have been recognized in HED meteorites (Fig. 7): Mg-rich olivine veinlets (Pang et al. 2017) and Fe-rich olivine veinlets (Takeda et al. 1983, 1994; Barrat et al. 2011; Roszjar et al. 2011; Mittlefehldt et al. 2013; Warren et al. 2014; Patzer and McSween 2018). The origin of these secondary olivine veinlets is still under

debate; multiple formation mechanisms have been proposed to account for veinlets in HED meteorites and lunar mare basalts. These are outlined below.

Shock-Induced Localized Melting Model

Pang et al. (2017) proposed that the shock-induced localized melting of forsteritic olivine ($\text{Fa}_{44.9-45.3}$) accounted for the formation of Mg-rich olivine veinlets with polycrystalline aggregates and highly irregular veinlet boundaries in eucrite NWA 1109 (Fig. 11a). Unlike this type of Mg-rich olivine veinlet, olivine veinlets in NWA 11273 show distinct textures (1) Mg-

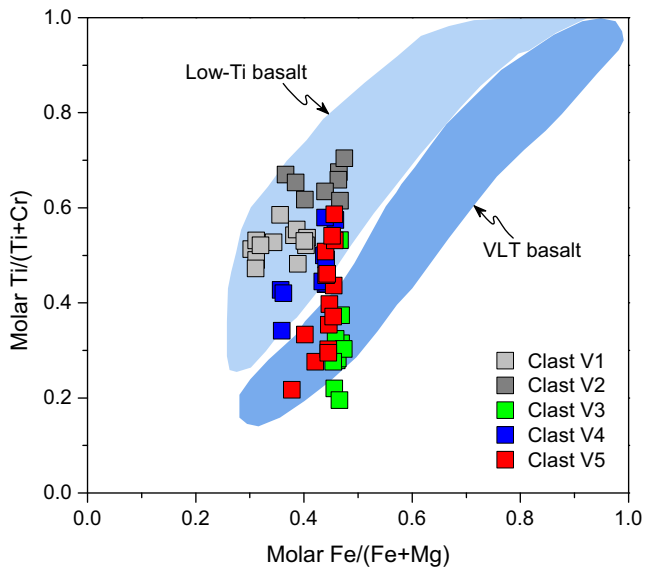


Fig. 10. Plot of molar $\text{Ti}/(\text{Ti}+\text{Cr})$ versus $\text{Fe}/(\text{Fe}+\text{Mg})$ for pyroxene in clasts V1–V5. Low-titanium (Low-Ti) basalt and very low-titanium (VLT) basalt fields are taken from Nielsen and Drake (1978) and Arai et al. (1996). (Color figure can be viewed at wileyonlinelibrary.com.)

rich olivine veinlets in eucrite NWA 1109 are observed connected with a relative large ($\sim 50 \mu\text{m}$) olivine crystal (fig. 8e of Pang et al. 2017), while olivine veinlets in NWA 11273 are not contiguous with other olivine grains; (2) olivine in some regions of NWA1109 occurs as polycrystalline aggregates (figs. 8c and 8d of Pang et al. 2017), which is a diagnostic feature of shock metamorphism. However, few shock features are observed in the olivine veinlet-bearing clasts within NWA 11273; and (3) the Mg-rich olivine veinlet-bearing clasts in eucritic NWA 1109 (i.e., clast-6; fig. 8 of Pang et al. 2017) contain FeNi metals with high Ni/Co ratios of 5–11, suggestive of meteoritic origin. In contrast, no FeNi metal was detected in the studied veinlet-bearing clasts V1–V5. These suggest that the impact-induced localized melting of phenocrystic olivine does not explain the formation of olivine veinlets in clasts V1–V5 of NWA 11273.

Textural relationships demonstrate that the studied olivine veinlets were not likely a typical primary crystallization product of clasts V1–V5's parental magma, but they are more likely to represent secondary filling of pyroxene grains that have previously been fractured by impact shock brittle deformation. One possible source of the secondary olivine veinlets in clasts V1–V5 is that they were crystallized from injection of a shock-induced silicate melt at high temperature ($\sim 1300 \text{ }^\circ\text{C}$; Médard and Grove 2007). If this scenario is correct, such silicate melt could percolate through clast V1–V5's parent rock along previously existing cracks

and grain boundaries, then locally forming the secondary olivine veinlets and other accessory minerals (i.e., plagioclase and chromite). However, the textures of secondary olivine veinlets in clasts V1–V5 are not consistent with this scenario. (1) Shock-induced melt veins in meteorites commonly cut through various mineral phases (e.g., Walton and Shaw 2009; Miyahara et al. 2013). In contrast, the studied olivine veinlets in NWA 11273 are only distributed in pyroxene crystals, but do not extend into the adjacent plagioclase (e.g., clast V2; Fig. 2d). Also, olivine veinlets in NWA 11273 were observed enclosed within host crystals (e.g., Figs. 2b and 3c), which are very texturally different from shock-induced melt veins. (2) A number of mineral phases (e.g., silicate grain, FeNi metal, troilite, and glass) are commonly observed in a shock-induced melt veins (e.g., Tomioka and Miyahara 2017; Zeng et al. 2018b). Such mineralogy is largely different in the mineral assemblages (i.e., olivine, plagioclase, and chromite) of olivine veinlets in NWA 11273. (3) If a shock-induced melt percolated cracks with clast V1–V5's parent rock, the temperature would have been too high ($\sim 1300 \text{ }^\circ\text{C}$) to form the wedge-shaped holes between olivine veinlets and surrounding pyroxene grains in clasts V1–V5 (Figs. 2–4). This is because some remelting of the host pyroxene would have likely occurred.

Remelting of Olivine Mesostasis and Incongruent Melting of Pyroxene Models

To account for the origin of Fe-rich olivine veinlets in HED meteorites, two possible mechanisms have been proposed; i.e., (1) shock-induced remelting of late-stage phases such as Fe-rich olivine mesostasis (Fig. 11b; Takeda et al. 1983, 1994) and (2) incongruent melting of primary pyroxene in the magma chamber (Fig. 11c; Roszjar et al. 2011). The further studies of HED meteorites have ruled out these two models (e.g., see the discussion in Pang et al. 2017). Likewise, applying this framework to lunar sample NWA 11273, these two models are difficult to account for the observed textural and mineralogical features in this meteorite as (1) we do not observe regions of mesostasis in any of the clasts V1–V5, the clasts themselves do not show excessive shock metamorphic textures (e.g., glassy veins), and the olivine veinlets are not seen in other mineral phases such as plagioclase (Figs. 2 and 3). All these textures imply that the shock-induced remelting model is not likely the formation mechanism of olivine veinlets in NWA 11273. (2) The incongruent melting of pyroxene model (Roszjar et al. 2011) is not consistent with the sharp boundaries between olivine veinlets and their host pyroxene grains in clasts V1–V5 (Figs. 2–4); if incongruent melting occurs, then a reaction texture

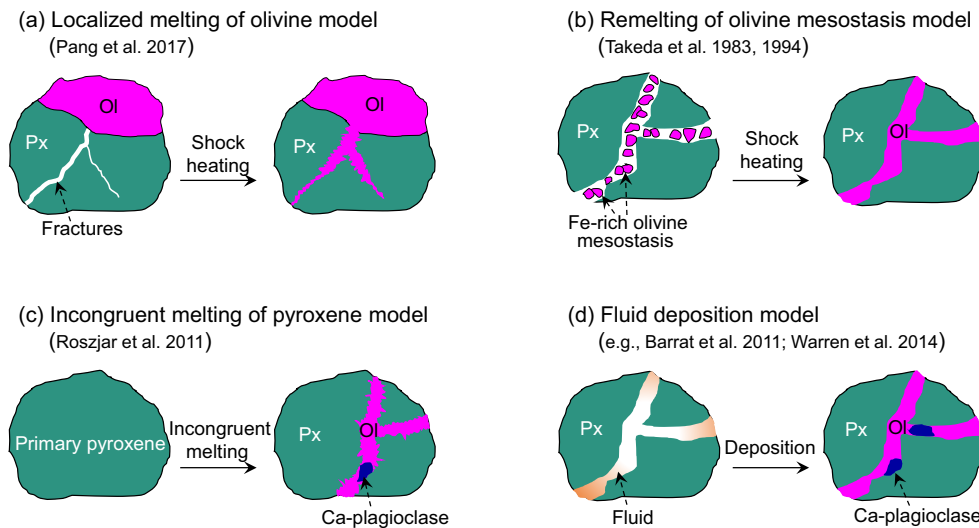


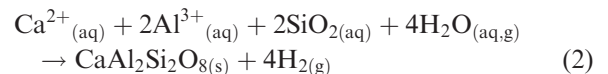
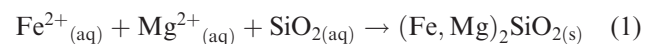
Fig. 11. Schematic showing existing models for explaining the olivine veinlets and their texture and mineral relationships seen in HED meteorites. (Color figure can be viewed at wileyonlinelibrary.com.)

would be expected at the boundaries of olivine veinlets and host pyroxene grains.

Fluid Deposition Model

Previous studies suggest that the fluid deposition model (Fig. 11d) is currently the most accepted model to explain the secondary Fe-rich olivine veinlets and associated Ca-plagioclase within veinlets in a series of HED meteorites (Barrat et al. 2011; Warren et al. 2014; Mittlefehldt 2015; Pang et al. 2017). Similar hydrothermally deposited fayalitic olivine (e.g., Rasmussen et al. 1998) and hydrothermally deposited anorthitic plagioclase (e.g., Python et al. 2007; Mora et al. 2009) are common on the Earth. Also, secondary fayalitic olivine that are related to fluid-mediated metasomatism have been described in many carbonaceous chondrite meteorites (e.g., Krot et al. 2000, 2002, 2004, 2007; Brearley and Krot 2013; Li et al. 2017). Recently, a fluid deposition model has also been used to explain the occurrence of olivine veinlets in lunar basalt 14072 (Warren et al. 2018). The reported olivine veinlets in lunar sample 14072 are similar to the olivine veinlets within NWA 11273 (1) olivine veins are widespread within pyroxene, but absent in plagioclase, (2) olivine veins have similar chemical composition (Fig. 6), and (3) both of them are associated with chromite grains. Accordingly, we have considered this process as the most likely mechanism for explaining the formation of secondary olivine veinlets in NWA 11273. The fluid deposition process can account for texture and mineralogy (e.g., irregular sharp boundaries) of the olivine veinlet-bearing clasts V1–V5.

In most cases, the fluid-driven metasomatism would occur along cracks or grain boundaries, resulting in dissolution or replacement of primary minerals (e.g., Krot et al. 2000, 2004; Shearer et al. 2012; Li et al. 2017; Warren et al. 2018; Zhang et al. 2018). However, the olivine veinlets in clasts V1–V5 are straight with sharp boundaries with their host pyroxene grains (Figs. 2–4). This suggests that olivine veinlets in NWA 11273 might not be a reaction product from the in situ replacement of their host pyroxene by fluids. These secondary olivine veinlets and associated plagioclase could have formed by direct deposition from the fluid percolating through the pyroxene fractures. This interpretation is further supported by the chemical composition difference between the secondary olivine veinlets and other olivine grains in NWA 11273 (Fig. 7). According to the fluid deposition model, the formation of secondary olivine veinlets with accessory anorthitic plagioclase can be interpreted by the general reaction: fluid \rightarrow olivine + Ca-plagioclase. Specifically, some type of aqueous fluid agent (i.e., water bearing) could transport the olivine/Ca-plagioclase cations (e.g., Fe^{2+} , Mg^{2+} , Si^{4+} , Ca^{2+} , and Al^{3+}) and then direct deposited the secondary minerals by the following reactions (Brearley and Krot 2013):



The absence of reaction boundaries in clasts V1–V5 suggests potentially relatively low temperature (<550 K)

for the formation of secondary olivine and Ca-plagioclase from aqueous solutions (Krot et al. 2004; Brearley and Krot 2013). In addition, the presence of wedge-shaped holes possibly suggests that the fluid contains a certain amount of volatile (e.g., H_2 as proposed in reaction 2).

In most circumstances, Cr^{3+} in hydrous fluid has low solubility and high immobility (Roeder and Reynolds 1991; Klein-Bendavid et al. 2011). This suggests that the small chromite grains sometimes found within the secondary olivine veinlets were more likely incorporated from their host pyroxene than formed in situ. In addition, pyroxene grains seen within secondary olivine veinlets have the same chemical composition as the host pyroxene (Table 2), suggesting that they could be the broken pieces of the host that have become mobilized by the fluid flow. This interpretation is supported by the irregular shape of pyroxene and chromite grains in olivine veinlets (Figs. 2 and 3). These irregular pyroxene and chromite grains are likely related to the brittle fracture of pyroxene, which was implicated by the observed wedge-shaped holes (Fig. 4a) and the irregular grain boundary (Figs. 2 and 3) of host pyroxene.

Consequently, the fluid deposition seems at present the most plausible candidate for explaining the secondary olivine veinlets in NWA 11273, although this model cannot readily account for certain textural observations such as the absence of olivine veinlets in other host mineral phases (e.g., plagioclase). Our studies and previous works have shown that olivine veinlets are commonly distributed in pyroxene crystals, but do not extend into the adjacent plagioclase (e.g., fig. 4 of Barrat et al. 2011; fig. 4 of Pang et al. 2017; figs. 1 and 2 of Warren et al. 2018). Pang et al. (2017) suggested that the lack of secondary olivine veins in plagioclase of HED meteorites is probably due to the different shock behavior of pyroxene and plagioclase, that is, the fractures could be widely developed in pyroxene, but are rare in plagioclase (e.g., fig. 4 of Chen and El Goresy 2000; fig. 2b of Zhang et al. 2011; fig. 2 of Ray et al. 2017; fig. 5e of Zeng et al. 2018b). This interpretation is consistent with our observations in clasts V1 and V2 that contain irregular crystalline pyroxene with fractures/cracks terminating at the boundaries of plagioclase grains (e.g., Fig. 2e).

Formation History of the Olivine Veinlet-Bearing Clasts in NWA 11273

NWA 11273 has bulk-rock composition similar to lunar highland feldspathic meteorites (Fig. 8), suggesting that the studied secondary olivine veinlets hosted in this meteorite are most likely to be formed in

lunar highland area. These olivine veinlets are restricted to individual lithic clasts and do not cut across the matrix surrounding the clasts (Figs. 2 and 3). This implies that these olivine veinlets were formed before the whole sample breccia-forming event.

The petrological and mineralogical features of clasts V1–V5 suggest that the formation of secondary olivine veinlets in NWA 11273 includes a variety of complex processes (see Fig. 12). (1) The basaltic host rocks of clasts V1–V5 were crystallized from an Fe-rich basaltic magma; (2) the basaltic host rocks experienced post-magmatic re-equilibration (e.g., the exsolution lamellae of clinopyroxene; Figs. 2 and 3) and also were shocked by an impact(s) to create a brittle fracture network; (3) fluids percolated through the host rock along these pre-existing fractures, forming irregular secondary olivine veinlets with accessory Ca-plagioclase grains; (4) many of the secondary olivine grains in clasts V1–V5 show 120° triple junction grain boundaries (e.g., Figs. 2e and 3b), suggesting that a later thermal metamorphic event of ~ 700 – $1000^\circ C$ occurred (temperatures estimated from the two-pyroxene thermometer of Lindsley and Andersen 1983; Figs. 6b–d). (5) Finally, the olivine veinlet-bearing host rock was impact ejected from their bedrock source, mixed with other lunar components (e.g., mineral fragments and highlands lithologies), and then consolidated to form a regolith breccia, which gave us meteorite NWA 11273.

Implications of the Secondary Olivine Veinlets in NWA 11273

In addition to the secondary olivine veinlets in highlands breccia NWA 11273, similar secondary olivine veinlets have also been previously observed in a few basaltic lunar samples (i.e., basaltic breccia meteorite MET 01210; Arai et al. 2010, and Apollo 14 mare basalt 14072; Warren et al. 2018). These findings imply that the formation mechanism for these olivine veinlets could be an underappreciated geological process within the lunar crust.

In HED meteorites, metasomatic system P- and S-bearing mineral phases (i.e., merrillite and troilite) have been detected associated with the secondary fayalitic olivine veinlets (e.g., Barrat et al. [2011] and references within; Pang et al. 2017). However, in this study, the secondary olivine veinlets in NWA 11273 were observed associated with only a few accessory mineral grains of chromite, pyroxene, and plagioclase (Figs. 2 and 3). The P-rich phases (e.g., phosphate) and S-rich minerals (e.g., troilite) were not detected in the olivine veinlet in clasts V1–V5 (Figs. 2 and 3; Table 1, see also Figs. S3.1–S3.5). This may indicate that the concentrations of P and S (or F and Cl, which are significant for the formation of the

mineral apatite; McCubbin et al. 2015) in the fluid that formed the secondary olivine in NWA 11273 (at least in clasts V1–V5) was relatively low.

In eucrite NWA 5738, Warren et al. (2014) observed a set of ferroan olivine and Ca-plagioclase curving microveins that are likely formed from aqueous-rich fluids (~700 °C). These authors indicated that the fluids could have come from an impactor that mobilized rock-forming elements (i.e., Fe, Mg, Si) from 4-Vesta target rocks, before re-precipitation occurred as veinlets (Warren et al. 2014). For the source of fluid related to secondary olivine veinlets in NWA 11273, it is possible that this fluid originated from an impactor (hydrated asteroid or comet); however, we favor a lunar origin for the fluids for the secondary olivine in NWA 11273. This is supported by the mineral composition (e.g., Fe/Mn ratios for mafic minerals and plagioclase composition) of the secondary olivine veinlets in NWA 11273, which are similar to the lunar samples (Figs. 5 and 7).

Metasomatic fluids have evidently played a complex role in different lunar magmatic systems. Lunar highland rocks show multiple lines of mineralogical and textural evidence for the metasomatism (e.g., Bell et al. 2015). For example, the observed sulfide replacement textures in Mg-Suite lithologies of lunar samples 67915 and 67016 are indicative of the presence of S-bearing fluid in lunar crust (Shearer et al. 2012; Bell et al. 2015). Dickinson et al. (1989) suggested that the source region for Apollo 14 aluminous mare basalts may have assimilated volatile-rich (Ge-rich) materials that had been metasomatized within the lunar mantle. In addition, during the thermal degassing of lunar regolith induced by the heat of emplaced basalts or nearby impact events, H-Cl-bearing volatile phases could have been released from the surface regolith to interact with the surface materials, modifying the δD and $\delta^{37}Cl$ signatures in lunar volcanic/magmatic samples (e.g., Greenwood et al. 2011; Tartèse et al. 2014; Pernet-Fisher 2016; Treiman et al. 2016; Potts et al. 2018). Taken together, these findings indicate that lunar metasomatic fluids were commonly enriched in volatiles (e.g., P, S, Ge, and Cl; McCubbin et al. 2015; Barnes et al. 2016a, 2016b; Potts et al. 2018), REE (Neal and Taylor 1991), and/or water/hydrogen (e.g., Barnes et al. 2014, 2016c; McCubbin et al. 2015; Robinson et al. 2016). However, the fluid responsible for the studied secondary olivine veinlets in NWA 11273 is significantly different from previous studies, as it is likely volatile element (e.g., S, P, or Cl) depleted.

In this study and previous investigations (e.g., Arai et al. 2010; Warren et al. 2018), only small amounts of microscale (<~30 μm in width) secondary olivine veinlets have been observed. The low abundances of veins identified in lunar samples indicate that fluid flow

was rare (and small scale) on the Moon. If a large amount of a fluid moved (flowed) through a rock, then larger portions of olivine veinlet-bearing clasts and larger scale (e.g., hundreds of microns to several millimeters in size) fluid deposited products would be expected. The existing sample collection gives a tantalizing hint of this poorly understood process. The upcoming Chang'e-5 sample return mission to the Mons Rumker and intermediate Ti mare basalt lava fields (Qian et al. 2018) provides a new opportunity to access new types of lavas and an evolved silicic volcanic dome. Future studies should be carried out to seek and characterize evidence of the past fluid mobility and deposition within these returned volcanic rocks in order to better relate the Moon's magmatic history to different volatile reservoirs and fluid mobility processes.

CONCLUSIONS

NWA 11273 is a feldspathic breccia, compositionally (e.g., $Al_2O_3 = 25.1$ wt%, Sm = 0.49 ppm, and Th = 0.17 ppm) similar to other lunar highland meteorites. In this sample, we have recognized five lithic pyroxene clasts that host secondary olivine veinlets (i.e., clasts V1–V5). These olivine veinlets cross cut their host pyroxene grains. They exhibit similar mineralogy to each other and are mainly composed of olivine with a few accessory mineral grains of chromite, pyroxene, and plagioclase. Compared with other olivine grains in lithic clasts and matrix of NWA 11273 ($FO_{54.3-83.1}$), the olivine veinlets in clasts V1–V5 are relatively fayalitic ($FO_{41.4-51.9}$). The mineralogy of clasts V1–V5 suggests that their host pyroxene represents basaltic lithologies, similar to low-Ti or VLT mare basalts.

By analogy with the secondary olivine veinlets observed in HED meteorite, the fluid deposition processes seem the most plausible mechanism for interpreting the formation of secondary olivine veinlets in NWA 11273. Petrological and mineralogical features of clasts V1–V5 reveal that formation history of secondary olivine veinlets in NWA 11273 includes a variety of complex processes; i.e., (1) the basaltic host rocks formed in lunar crust, (2) postmagmatic re-equilibration and fracturing by impact events, (3) secondary veinlets were formed by deposition from metasomatic fluid, and (4) NWA 11273 was consolidated with the olivine veinlet-bearing clasts (Fig. 12).

The observed secondary olivine veinlets in NWA 11273 may be evidence of fluid deposition at or close to the lunar surface. On the basis of the currently available data, we propose that such fluid was likely S,P-poor and was from an endogenic origin on the Moon. To better understand the formation mechanism of secondary olivine veinlets on the Moon, more olivine

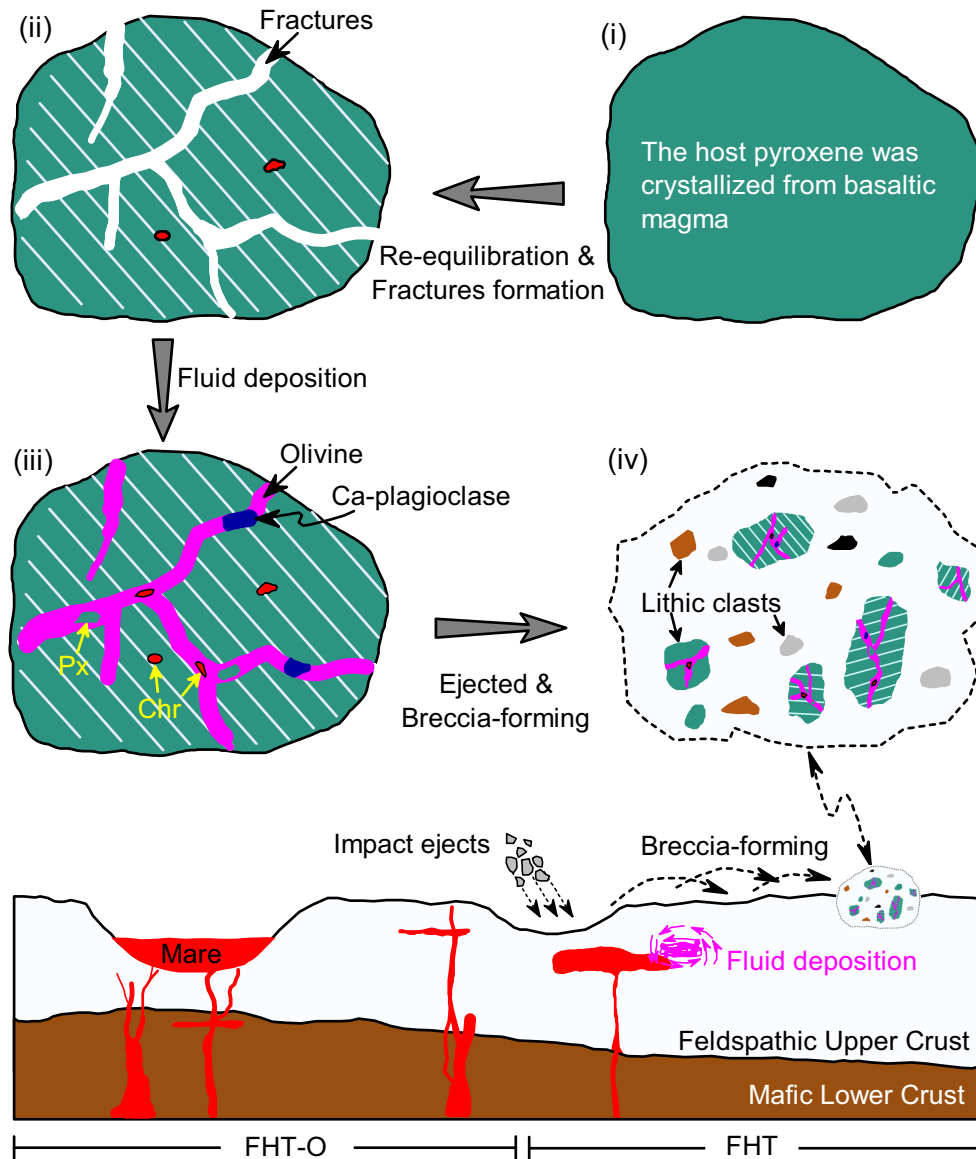


Fig. 12. Cartoon illustrating the highland origin of NWA 11273 and the formation history of olivine veinlet-bearing clasts within basaltic magmas. (Color figure can be viewed at wileyonlinelibrary.com.)

veinlet-bearing lunar clasts are need to be examined and comparative studies of olivine veinlets between lunar samples (such as those that will be collected by the upcoming Chang'e-5 mission) and HED meteorites are also necessary. In addition, the systematic studies of in situ oxygen isotope and trace elements, in the future, would allow for greater revealing the geological records of such secondary olivine veinlets in lunar samples.

Acknowledgments—We thank Hao Zhu (Beijing Planetarium) for donating lunar meteorite NWA 11273. We thank Chris Herd for the editorial handling and two anonymous reviewers for their constructive comments

on an earlier version of this manuscript. We also thank Dr. Fagan and an anonymous reviewer for their fruitful comments, as well as Dr. Righter for editorial handling. X.Z. thank YiZhi Liu and Yan Zhong for their help during the EMPA measurements at the Guilin University of Technology. This work was financially supported by the National Natural Science Foundation of China (nos 41473067, 41490630, 41572037, and 41941003) and Key Research Program of the Chinese Academy of Sciences (XDPB11). J.Z.L. acknowledges the Key Program of Frontier Science of Chinese Academy of Sciences (QYZDY-SSW-DQC028). K.H.J. acknowledges funding from Royal Society grant RS/

UF140190, STFC grant ST/R000751/1, Leverhulme Trust grant RPG-2019-222, and to the Chinese Academy of Sciences for facilitating a research visit to the Institute of Geochemistry.

Editorial Handling—Dr. Kevin Righter

REFERENCES

- Agarwal A., Reznik B., Alva-Valdivia L. M., and Srivastava D. C. 2017. Alternating augite-plagioclase wedges in basement dolerites of Lockne impact structure, Sweden: A new shock wave-induced deformation feature. *Meteoritics & Planetary Science* 52:458–470.
- Al-Kathiri A., Hofmann B. A., Jull A. J. T., and Gnos E. 2005. Weathering of meteorites from Oman: Correlation of chemical and mineralogical weathering proxies with ^{14}C terrestrial ages and the influence of soil chemistry. *Meteoritics & Planetary Science* 40:1215–1239.
- Anders E. and Grevesse N. 1989. Abundances of the elements—Meteoritics and solar. *Geochimica et Cosmochimica Acta* 53:197–214.
- Arai T., Takeda H., and Warren P. H. 1996. Four lunar mare meteorites: Crystallization trends of pyroxenes and spinels. *Meteoritics & Planetary Science* 31:877–892.
- Arai T., Hawke B. R., Giguere T. A., Misawa K., Miyamoto M., and Kojima H. 2010. Antarctic lunar meteorites Yamato-793169, Asuka-881757, MIL 05035, and MET 01210 (YAMM): Launch pairing and possible cryptomare origin. *Geochimica et Cosmochimica Acta* 74:2231–2248.
- Barnes J. J., Tartèse R., Anand M., McCubbin F. M., Franchi I. A., Starkey N. A., and Russell S. S. 2014. The origin of water in the primitive Moon as revealed by the lunar highlands samples. *Earth and Planetary Science Letters* 390:244–252.
- Barnes J. J., Mahesh A., and Franchi I. A. 2016a. Investigating the history of magmatic volatiles in the moon using nanosims. *Microscopy & Microanalysis* 22:1804–1805.
- Barnes J. J., Tartèse R., Anand M., McCubbin F. M., Neal C. R., and Franchi I. A. 2016b. Early degassing of lunar urkreep by crust-breaching impact(s). *Earth and Planetary Science Letters* 447:84–94.
- Barnes J. J., Kring D. A., Tartèse R., Franchi I. A., Anand M., and Russell S. S. 2016c. An asteroidal origin for water in the moon. *Nature Communications* 7:11684.
- Barrat J. A., Yamaguchi A., Bunch T. E., Bohn M., Bollinger C., and Ceuleneer G. 2011. Possible fluid–rock interactions on differentiated asteroids recorded in eucritic meteorites. *Geochimica et Cosmochimica Acta* 75:3839–3852.
- Bell A. S., Shearer C., Demoor J. M., and Provencio P. 2015. Using the sulfide replacement petrology in lunar breccia 67915 to construct a thermodynamic model of S-bearing fluid in the lunar crust. *Geochimica et Cosmochimica Acta* 171:50–60.
- Binder A. B. 1998. Lunar prospector: Overview improved gravity field of the moon from lunar prospector. *Science* 281:1475–1476.
- Boyce J. W., Liu Y., Rossman G. R., Guan Y., Eiler J. M., Stolper E. M., and Taylor L. A. 2010. Lunar apatite with terrestrial volatile abundances. *Nature* 466:466–469.
- Brearley A. J. and Krot A. N. 2013. Metasomatism in the early solar system: The record from chondritic meteorites. In *Metasomatism and the chemical transformation of rock*, edited by Harlov D. E. and Austrheim H. Berlin: Springer. pp. 659–789.
- Cahill J., Floss C., Anand M., Taylor L. A., Nazarov M. A., and Cohen B. A. 2004. Petrogenesis of lunar highlands meteorites: Dhofar 025, Dhofar 081, Dar al Gani 262, and Dar al Gani 400. *Meteoritics & Planetary Science* 39:503–529.
- Calzada-Diaz A., Joy K. H., Crawford I. A., and Nordheim T. A. 2015. Constraining the source regions of lunar meteorites using orbital geochemical data. *Meteoritics & Planetary Science* 50:214–228.
- Chen M. and El Goresy A. 2000. The nature of maskelynite in shocked meteorites: Not diaplectic glass but a glass quenched from shock-induced dense melt at high pressures. *Earth and Planetary Science Letters* 179:489–502.
- Colson R. O. 1992. Mineralization on the Moon? Theoretical considerations of Apollo 16 “rusty rocks,” replacement in 67016, and surface-correlated volatiles on lunar volcanic glass. Proceedings, 22nd Lunar and Planetary Science Conference. pp. 427–436.
- Day J. M. D., Floss C., Taylor L. A., Anand M., and Patchen A. D. 2006. Evolved mare basalt magmatism, high Mg/Fe feldspathic crust, chondritic impactors, and the petrogenesis of Antarctic lunar breccia meteorites Meteorite Hills 01210 and Pecora Escarpment 02007. *Geochimica et Cosmochimica Acta* 70:5957–5989.
- Dickinson T., Taylor G. J., Keil K., and Bild R. W. 1989. Germanium abundances in lunar basalts—Evidence of mantle metasomatism? Proceedings, 19th Lunar and Planetary Science Conference. pp. 189–198.
- Elardo S. M., McCubbin F. M., and Shearer C. K. 2012. Chromite symplectites in Mg-suite troctolite 76535 as evidence for infiltration metasomatism of a lunar layered intrusion. *Geochimica et Cosmochimica Acta* 87:154–177.
- Fagan T. J., Kashima D., Wakabayashi Y., and Suginozono A. 2014. Case study of magmatic differentiation trends on the Moon based on lunar meteorite Northwest Africa 773 and comparison with Apollo 15 quartz monzodiorite. *Geochimica et Cosmochimica Acta* 133:97–127.
- Greenwood J. P., Itoh S., Sakamoto N., Warren P., Taylor L., and Yurimoto H. 2011. Hydrogen isotope ratios in lunar rocks indicate delivery of cometary water to the Moon. *Nature Geoscience* 4:79–82.
- Haskin L. A. and Warren P. 1991. Lunar chemistry. In *Lunar source book*, edited by Heiken G. H., Vaniman D. T., and French B. V. New York: Cambridge University Press. pp. 357–474.
- Hauri E. H., Weinreich T., Saal A. E., Rutherford M. C., and Van Orman J. A. 2011. High pre-eruptive water contents preserved in lunar melt inclusions. *Science* 333:213–215.
- Hui H., Peslier A. H., Zhang Y., and Neal C. R. 2013. Water in lunar anorthosites and evidence for a wet early Moon. *Nature Geoscience* 6:177–180.
- Hyde B. C., Day J. M. D., Tait K. T., Ash R. D., Holdsworth D. W., and Moser D. E. 2014. Characterization of weathering and heterogeneous mineral phase distribution in brachinite northwest Africa 4872. *Meteoritics & Planetary Science* 49:1141–1156.
- Isa J., Warren P. H., Rubin A. E., McKeegan K. D., and Gessler N. 2014. Fluid deposition products in eucrites and

- moon rocks: A study in contrasts (abstract #2777). 45th Lunar and Planetary Science Conference. CD-ROM.
- Jolliff B. L., Gillis J. J., Haskin L. A., Korotev R. L., and Wieczorek M. A. 2000. Major lunar crustal terranes: Surface expressions and crust-mantle origins. *Journal of Geophysical Research* 105:4197–4216.
- Joy K. H., Crawford I. A., Russell S. S., and Kearsley A. T. 2010. Lunar meteorite regolith breccias: An in situ study of impact melt composition using LA-ICP-MS with implications for the composition of the lunar crust. *Meteoritics & Planetary Science* 45:917–946.
- Joy K. H., Zolensky M. E., Nagashima K., Huss G. R., McKay D. S., Ross D. K., and Kring D. A. 2012. Direct detection of projectile relics from the end of the lunar basin-forming epoch. *Science* 336:1426–1429.
- Joy K. H., Nemchin A., Grange M., Lapen T. J., Peslier A. H., Ross D. K., Zolensky M. E., and Kring D. A. 2014. Petrography, geochronology and source terrain characteristics of lunar meteorites Dhofar 925, 961 and Sayh al Uhaymir 449. *Geochimica et Cosmochimica Acta* 144:299–325.
- Joy K. H., Crawford I. A., Curran N. M., Zolensky M., Fagan A. F., and Kring D. A. 2016. The Moon: An archive of small body migration in the solar system. *Earth Moon and Planets* 118:133–158.
- Klein-Bendavid O., Pettke T., and Kessel R. 2011. Chromium mobility in hydrous fluids at upper mantle conditions. *Lithos* 125:122–130.
- Korotev R. L. 1997. Some things we can infer about the moon from the composition of the Apollo 16 regolith. *Meteoritics & Planetary Science* 32:447–478.
- Korotev R. L. 2005. Lunar geochemistry as told by lunar meteorites. *Chemie der Erde — Geochemistry* 65:297–346.
- Korotev R. L., Jolliff B. L., Zeigler R. A., Gillis J. J., and Haskin L. A. 2003. Feldspathic lunar meteorites and their implications for compositional remote sensing of the lunar surface and the composition of the lunar crust. *Geochimica et Cosmochimica Acta* 67:4895–4923.
- Korotev R. L., Zeigler R. A., and Jolliff B. L. 2006. Feldspathic lunar meteorites pecora escarpment 02007 and Dhofar 489: Contamination of the surface of the lunar highlands by post-basin impacts. *Geochimica et Cosmochimica Acta* 70:5935–5956.
- Krot A. N., Brearley A. J., Petaev M. I., Kallemeyn G. W., Sears D. W., Benoit P. H., Hutcheon I. D., Zolensky M. E., and Keil K. 2000. Evidence for low-temperature growth of fayalite and hedenbergite in MacAlpine Hills 88107, an ungrouped carbonaceous chondrite related to the CM-CO clan. *Meteoritics & Planetary Science* 35:1365–1386.
- Krot A. N., Hutcheon I. D., and Keil K. 2002. Plagioclase-rich chondrules in the reduced CV chondrites: Evidence for complex formation history and genetic links between calcium-aluminum-rich inclusions and ferromagnesian chondrules. *Meteoritics & Planetary Science* 37:155–182.
- Krot A. N., Petaev M. I., and Bland P. A. 2004. Multiple formation mechanisms of ferrous olivine in Cv carbonaceous chondrites during fluid-assisted metamorphism. *Antarctic Meteorite Research* 17:153.
- Krot A. N., Yurimoto H., Hutcheon I. D., Libourel G., Chaussidon M., Tissandier L., Petaev M. I., MacPherson G. J., Paque-Heather J., and Wark D. 2007. Type C Ca, Al-rich inclusions from Allende: Evidence for multistage formation. *Geochimica et Cosmochimica Acta* 71:4342–4364.
- Laul J. C., Smith M. R., and Schmitt R. A. 1983. ALHA 81005 meteorite: Chemical evidence for lunar highland origin. *Geophysical Research Letters* 10:825–828.
- Lawrence D. J., Feldman W. C., Elphic R. C., Little R. C., Prettyman T. H., Maurice S., Lucey P. G., and Binder A. B. 2002. Iron abundances on the lunar surface as measured by the Lunar Prospector gamma-ray and neutron spectrometers. *Journal of Geophysical Research* 107:5130.
- Lawrence D. J., Elphic R. C., Feldman W. C., Prettyman T. H., Gasnault O., and Maurice S. 2003. Small-area thorium features on the lunar surface. *Journal of Geophysical Research* 108:5102.
- Lee M. R. and Bland P. A. 2004. Mechanisms of weathering of meteorites recovered from hot and cold deserts and the formation of phyllosilicates. *Geochimica et Cosmochimica Acta* 68:893–916.
- Li Y., Zhang A. C., Chen J. N., Gu L. X., and Wang R. C. 2017. Formation of phosphorus-rich olivine in Dar al Gani 978 carbonaceous chondrite through fluid-assisted metamorphism. *American Mineralogist* 102:98–107.
- Lindsley D. H. and Andersen D. J. 1983. A two-pyroxene thermometer. *Journal of Geophysical Research: Solid Earth* 88:A887–A906.
- Lorenzetti S., Busemann H., and Eugster O. 2005. Regolith history of lunar meteorites. *Meteoritics & Planetary Science* 40:315–327.
- Lucey P., Korotev R. L., Gillis J. J., Taylor L. A., Lawrence D., Campbell B. A., Elphic R., Feldmann B., Hood L. L., Hunten D., Mendillo M., Noble S., Papike J. J., Reedy R. C., Lawson S., Prettyman T., Gasnault O., and Maurice S. 2006. Understanding the lunar surface and space-Moon interactions. In *New views of the Moon*, edited by Jolliff B. L., Wieczorek M. A., Shearer C. K., and Neal C. R. *Reviews in Mineralogy and Geochemistry* 60:83–219.
- Mccallum I. S. and Schwartz J. M. 2001. Lunar mg suite: Thermobarometry and petrogenesis of parental magmas. *Journal of Geophysical Research (Planets)* 106:27,969–27,983.
- McCubbin F. M., Vander Kaaden K. E., Tartèse R., Klima R. L., Liu Y., Mortimer J., Barnes J. J., Shearer C. K., Treiman A. H., Lawrence D. J., Elardo S. M., Hurley D. M., Boyce J. W., and Anand M. 2015. Magmatic volatiles (H, C, N, F, S, Cl) in the lunar mantle, crust, and regolith: Abundances, distributions, processes, and reservoirs. *American Mineralogist* 100:1668–1707.
- Médard E., and Grove T. L. 2007. Water in basaltic melts: Effect on liquidus temperatures, olivine-melt thermometry and mantle melting. The Workshop on Water in Planetary Basalts (Vol. 1373). Workshop on Water in Planetary Basalts.
- Mercer C. N., Treiman A. H., and Joy K. H. 2013. New lunar meteorite Northwest Africa 2996: A window into farside lithologies and petrogenesis. *Meteoritics & Planetary Science* 48:289–315.
- Mittlefehldt D. W. 2015. Asteroid (4) Vesta: I. the howardite-eucrite-diogenite (HED) clan of meteorites. *Chemie der Erde — Geochemistry* 75:155–183.
- Mittlefehldt D. W., Herrin J. S., Quinn J. E., Mertzman S. A., Cartwright J. A., Mertzman K. R., and Peng Z. X. 2013. Composition and petrology of HED polymict breccias:

- The regolith of (4) Vesta. *Meteoritics & Planetary Science* 48:2105–2134.
- Miyahara M., Kaneko S., Ohtani E., Sakai T., Nagase T., Kayama M., Nishido H., and Hirao N. 2013. Discovery of seifertite in a shocked lunar meteorite. *Nature Communications* 4:1737.
- Mora C. I., Riciputi L. R., Cole D. R., and Walker K. D. 2009. High-temperature hydrothermal alteration of the boehls butte anorthosite: origin of a bimodal plagioclase assemblage. *Contributions to Mineralogy and Petrology* 157:781–795.
- Neal C. R. and Taylor L. A. 1991. Evidence for metasomatism of the lunar highlands and the origin of whitlockite. *Geochimica et Cosmochimica Acta* 55:2965–2980.
- Nielsen R. L. and Drake M. J. 1978. The case for at least three mare basalt magmas at the Luna 24 landing site. In *Mare Crisium: The view from Luna 24*, edited by Merrill R. B. and Papike J. J. New York: Pergamon Press. pp. 419–428.
- Norman M. D., Keil K., Griffin W. L., and Ryan C. G. 1995. Fragments of ancient lunar crust: Petrology and geochemistry of ferroan noritic anorthosites from the Descartes region of the Moon. *Geochimica et Cosmochimica Acta* 59:831–847.
- Pang R. L., Zhang A. C., and Wang R. C. 2017. Complex origins of silicate veinlets in HED meteorites: A case study of Northwest Africa 1109. *Meteoritics & Planetary Science* 52:2113–2131.
- Papike J. J., Karner J. M., Shearer C. K., and Burger P. V. 2009. Silicate mineralogy of Martian meteorites. *Geochimica et Cosmochimica Acta* 73:7443–7485.
- Patzer A. and McSween M. S. 2018. Ferroan olivine-bearing eucrite clasts found in howardites. *Meteoritics & Planetary Science* 53:1131–149.
- Pernet-Fisher J. F. 2016. New evidence for lunar basalt metasomatism by underlying regolith. *American Mineralogist* 101:1497–1498.
- Potts N. J., Barnes J. J., Tartèse R., Franchi I. A., and Anand M. 2018. Chlorine isotopic compositions of apatite in Apollo 14 rocks: Evidence for widespread vapor-phase metasomatism on the lunar nearside ~ 4 billion years ago. *Geochimica et Cosmochimica Acta* 230:46–59.
- Python M., Ceuleneer G., Ishida Y., Barrat J. A., and Arai S. 2007. Oman diopsidites: A new lithology diagnostic of very high temperature hydrothermal circulation in mantle peridotite below oceanic spreading centres. *Earth and Planetary Science Letters* 255:289–305.
- Qi L., Hu J., and Gregoire D. C. 2000. Determination of trace elements in granites by inductively coupled plasma mass spectrometry. *Talanta* 51:507–513.
- Qian Y. Q., Xiao L., Zhao S. Y., Zhao J. N., Huang J., Flahaut J., Martinot M., Head J.W., Hiesinger H., and Wang G. X. 2018. Geology and scientific significance of the Rümker Region in Northern Oceanus Procellarum: China's Chang'E-5 landing region. *Journal of Geophysical Research: Planets* 123:1407–1430.
- Rasmussen M. G., Evans B. W., and Kuehner S. M. 1998. Low temperature fayalite, greenalite, and minnesotaite from the overlook gold deposits, Washington; phase relations in the system FeO-SiO₂-H₂O. *Canadian Mineralogist* 36:147–162.
- Ray D., Ghosh S., and Murty S. V. S. 2017. On the possible origin of troilite-metal nodules in the Katol chondrite (L6-7). *Meteoritics & Planetary Science* 52:72–88.
- Robinson K. L., Barnes J. J., Nagashima K., Thomen A., Franchi I. A., Huss G. R., Anand M., and Taylor G. J. 2016. Water in evolved lunar rocks: Evidence for multiple reservoirs. *Geochimica et Cosmochimica Acta* 188:244–260.
- Roedder E. and Weiblen P. W. 1972. Petrographic features and petrologic significance of melt inclusions in Apollo 14 and 15 rocks. Proceedings, 3rd Lunar and Planetary Science Conference Proceedings. 251.
- Roeder P. L. and Reynolds I. 1991. Crystallization of chromite and chromium solubility in basaltic melts. *Journal of Petrology* 32:909–934.
- Roszar J., Metzler K., Bischoff A., Barrat J. A., Geisler T. G., Greenwood R. C., Franchi I. A., and Klemme S. 2011. Thermal history of Northwest Africa 5073—A coarse grained Stannern-trend eucrite containing cm-sized pyroxenes and large zircon grains. *Meteoritics & Planetary Science* 46:1754–1773.
- Saal A. E., Hauri E. H., Cascio M. L., Van Orman J. A., Rutherford M. C., and Cooper R. F. 2008. Volatile content of lunar volcanic glasses and the presence of water in the Moon's interior. *Nature* 454:192–195.
- Saunier G., Poitrasson F., Moine B., Gregoire M., and Seddiki A. 2010. Effect of hot desert weathering on the bulk-rock iron isotope composition of L6 and H5 ordinary chondrites. *Meteoritics & Planetary Science* 45:195–209.
- Shearer C. K., Burger P. V., Guan Y., Papike J. J., Sutton S. R., and Atudorei N. V. 2012. Origin of sulfide replacement textures in lunar breccias. Implications for vapor element transport in the lunar crust. *Geochimica et Cosmochimica Acta* 83:138–158.
- Snape J. F., Joy K. H., and Crawford I. A. 2011. Characterization of multiple lithologies within the lunar feldspathic regolith breccia meteorite Northeast Africa 001. *Meteoritics & Planetary Science* 46:1288–1312.
- Sokol A. K., Fernandes V. A., Schulz T., Bischoff A., Burgess R., Clayton R. N., Munker C., Nishiizumi K., Palme H., Schultz L., Weckwerth G., Mezger K., and Horstmann M. 2008. Geochemistry, petrology and ages of the lunar meteorites Kalahari 008 and 009: New constraints on early lunar evolution. *Geochimica et Cosmochimica Acta* 72:4845–4873.
- Stöffler D., Ryder G., Ivanov B. A., Artemieva N. A., Cintala M. J., and Grieve R. A. 2006. Cratering history and lunar chronology. *Reviews in Mineralogy and Geochemistry* 60:519–596.
- Takeda H., Mori H., Wooden J. L., Nyquist L. E., Delaney J. S., and Prinz M. 1983. Comparison of Yamato and Victoria Land polymict eucrites—A view from mineralogical and isotopic studies. Proceedings, 14th Lunar and Planetary Science Conference. pp. B245–B246.
- Takeda H., Mori H. and Bogard D. D. 1994. Mineralogy and ³⁹Ar-⁴⁰Ar age of an old pristine basalt: Thermal history of the HED parent body. *Earth and Planetary Science Letters* 122:183–194.
- Tartèse R., Anand M., Barnes J. J., Starkey N. A., Franchi I. A., and Sano Y. 2013. The abundance, distribution, and isotopic composition of hydrogen in the Moon as revealed by basaltic lunar samples: Implications for the volatile inventory of the Moon. *Geochimica et Cosmochimica Acta* 122:58–74.
- Tartèse R., Anand M., Mccubbin F. M., Elardo S. M., Shearer C. K., and Franchi I. A. 2014. Apatites in lunar KREEP basalts: The missing link to understanding the h isotope systematics of the moon. *Geology* 42:363–366.

- Tomioka N. and Miyahara M. 2017. High-pressure minerals in shocked meteorites. *Meteoritics & Planetary Science* 52:2017–2039.
- Treiman A. H., Boyce J. W., Gross J., Guan Y., Eiler J. M., and Stolper E. M. 2014. Phosphate-halogen metasomatism of lunar granulite 79215: Impact-induced fractionation of volatiles and incompatible elements. *American Mineralogist* 99:1860–1870.
- Treiman A. H., Boyce J. W., Greenwood J. P., Eiler J. M., Gross J., Guan Y., Ma C., and Stolper E. M. 2016. D-poor hydrogen in lunar mare basalts assimilated from lunar regolith. *American Mineralogist* 101:1596–1603.
- Velbel M. A. 2014. Terrestrial weathering of ordinary chondrites in nature and continuing during laboratory storage and processing: Review and implications for Hayabusa sample integrity. *Meteoritics & Planetary Science* 49:154–171.
- Walton E. L. and Shaw C. S. 2009. Understanding the textures and origin of shock melt pockets in Martian meteorites from petrographic studies, comparisons with terrestrial mantle xenoliths, and experimental studies. *Meteoritics & Planetary Science* 44:55–76.
- Warren P. H. 2002. Northwest Africa 1000: A new eucrite with maskelynite, unequilibrated pyroxene crisscrossed by fayalite-rich veins and Stannern-like geochemistry (abstract #1147). 33rd Lunar and Planetary Science Conference. CD-ROM.
- Warren P. H., Ulf-Møller F., and Kallemeyn G. W. 2005. “New” lunar meteorites: Impact melt and regolith breccias and large-scale heterogeneities of the upper lunar crust. *Meteoritics & Planetary Science* 40:989–1014.
- Warren P. H., Rubin A. E., Isa J., Gessler N., Ahn I., and Choi B. G. 2014. Northwest Africa 5738: Multistage fluid driven secondary alteration in an extraordinarily evolved eucrite. *Geochimica et Cosmochimica Acta* 141:199–227.
- Warren P. H., Esposito R., and Manning C. 2018. Secondary, aqueous (?), metasomatic olivine veins in Apollo 14 mare basalt 1472 (abstract #2747). 49th Lunar and Planetary Science Conference. CD-ROM.
- Wittmann A., Korotev R. L., Jolliff B. L., Lapen T. J., and Irving A. J. 2014. The petrogenesis of impact basin melt rocks in lunar meteorite Shir 161. *American Mineralogist* 99:1626–1647.
- Yamaguchi A., Taylor G. J., and Keil K. 1996. Global crustal metamorphism of the eucrite parent body. *Icarus* 124:97–112.
- Yamaguchi A., Karouji Y., Takeda H., Nyquist L., Bogard D., Ebihara M., Shih C.-Y., Reese Y., Garrison D., Park J., and McKay G. 2010. The variety of lithologies in the Yamato-86032 lunar meteorite: Implications for formation processes of the lunar crust. *Geochimica et Cosmochimica Acta* 74:4507–4530.
- Zeng X., Joy K. H., Li S., Pernet-Fisher J. F., Li X., Martin D. J. P., and Wang S. 2018a. Multiple lithic clasts in lunar breccia Northwest Africa 7948 and implication for the lithologic components of lunar crust. *Meteoritics & Planetary Science* 53:1030–1050.
- Zeng X., Li S., Leya I., Wang S., Smith T., Li Y., and Wang P. 2018b. The Kumtag 016 L5 strewn field, Xinjiang Province, China. *Meteoritics & Planetary Science* 53:1113–1130.
- Zhang A. C. and Hsu W. 2009. Petrography, mineralogy, and trace element geochemistry of lunar meteorite Dhofar 1180. *Meteoritics & Planetary Science* 44:1265–1286.
- Zhang A. C., Hsu W. B., Floss C., Li X. H., Li Q. L., Liu Y., and Taylor L. A. 2011. Petrogenesis of lunar meteorite Northwest Africa 2977: Constraints from in situ microprobe results. *Meteoritics & Planetary Science* 45:1929–1947.
- Zhang A. C., Bu Y. F., Pang R. L., Sakamoto N., Yurimoto H., Chen L. H., Gao J. F., Du D. H., Wang X. L., and Wang R. C. 2018. Origin and implications of troilite-orthopyroxene intergrowths in the brecciated diogenite Northwest Africa 7183. *Geochimica et Cosmochimica Acta* 220:125–145.

SUPPORTING INFORMATION

Additional supporting information may be found in the online version of this article:

Fig. S1. Scan image of five studied NWA 11273 sections.

Figs. S2.1–2.5. BSE images of the lunar feldspathic meteorite NWA 11273, containing the studied clasts V1–V5.

Figs. S3.1–3.5. The BSE image and X-ray elemental mapping results for clasts V1–V5.

Table S1. The mineral composition of the olivine veinlet-bearing clasts V1–V5 in NWA 11273.

Table S2. The measured and reference values of reference materials for ICP-MS analysis.

Table S3. The measured and reference values of reference materials for ICP-OES analysis